NASA Technical Memorandum 101007

SIRTF Nod Maneuvers

N. Rajan

August 1988

National Aeronautics and
Space Administration

NASA Technical Memorandum 101007

SIRTF Nod Maneuvers

N. Rajan, Ames Research Center, Moffett Field, California

August 1988

National Aeronautics and
Space Administration

Ames Research Center
Moffett Field, California 94035

SUMMARY

The response of the Space Infrared Telescope Facility's attitude control system to a nod command is studied under a wide variety of conditions. Several engineering issues are explored: the effects of variations in the structural model, relocation of sensors and actuators, the influence of the fine-guidance-sensor sampling period, resolution and noise on the system response, torque and rate-integrating gyro noise and disturbances. Simulation results using control-moment gyros and reaction wheels as actuators are presented.

SIRTF NOD MANEUVERS

Introduction

During the latter half of 1987 and early into 1988, the nod maneuver for SIRTF was extensively investigated, using both analysis techniques and computer simulation. The first aim of the investigation was to set up an independent in-house analysis and simulation capability and to corroborate the earlier results reported in reference 1 and by F. H. Bauer and A. K. Birky in the NASA Goddard Flight Center, Guidance and Control Branch, Report 341, October 1985. Once this was achieved, however, the focus changed to exploring the various engineering issues involved in system performance and stability, using the nod maneuver as a vehicle. The nod maneuver was perceived to be representative of the system performance as it needs to be executed under various conditions, with and without the fine guidance sensor (FGS), for example. Besides it makes severe demands on the system in terms of the time response.

In PD 1011, the requirements document for SIRTF, nodding is defined as a sequence of small angle slew maneuvers "in alternating opposite directions." The "nods" in the present report are individual maneuvers in the previous sequence.

The engineering issues that can be answered via the currently available analysis/simulation setup are the following:

a. What are the structural model features that limit the nod response speed, enforce the design of a special compensator and make the controller nonrobust? Can the situation be improved by increasing structural damping coefficients, by changing the locations of the actuators and sensors or in some way moving the modal frequencies? Insensitivity to parameter variations, or robustness, is part of this issue.

b. How do the FGS parameters affect the system performance? The specific parameters of interest are the following: sampling rate, resolution, field of view, time delay, and noise. A further complication is where the FGS output represents an average position over the sampling interval.

c. What is the best method of executing the nod maneuver? Is "feedforward" torquing followed by loop closure preferable to closed-loop maneuvering? Is the command profile to be sine-versine or sawtooth? At what stage of a maneuver should the FGS be switched on? Are Control Moment Gyros (CMG) essential for performing the nod within 20 sec? Are CMGs alone adequate or is a combination of CMG and Reaction Wheels (RW) necessary?

d. How much is the performance degraded by these phenomena? The observatory is subject to ADR, gravity gradient, radiation pressure, RW and CMG mass unbalance and ripple as torque disturbances. The other major error source is the Rate-Integrating-Gyro (RIG) with both bias and random aberrations. Thermal bending of the structure contributes an equivalent attitude error from the RIG.

e. Can redesign of the PID gains or a change in the basic control algorithm lead to an improvement in the speed of response? What are the implementation aspects of such a change in terms of system software?

The currently available analysis and simulation results are described against the background of the above issues. First, the mathematical model employed in the investigations is briefly outlined.

System Model

All the control system studies conducted inhouse have employed the end- mounted spacecraft model called the flexible telescope model(FTM) in the report by Bauer and Birky (NASA Goddard Space Flight Center, Guidance and Control Branch, Report 341, October 1985).

Figure 1 shows a system block diagram. The observatory model is the single-axis FTM of Bauer and Birky. The control algorithm is proportional-integral and derivative (PID) with a second-order observer (table 1 gives controller parameter values for the **baseline** controller). A single-axis study is representative of the more detailed three-axis model where the inertial coupling between axes is small and the angular rates during maneuvers are "low." The inertial cross-coupling is directly related to the products of inertia; these are seen to be quite small compared to the moments of inertia (table 2). The effect of angular rates on any given axis, is proportional to the product of the rates in the other two axes and is, hence, small.

The structural modes retained in the simulation model are shown together with their physical description in table 3. Starting with the 20 modes used in the Goddard study, the number of modes was reduced to eight based upon a comparison of the open-loop poles and zeros. (Simulation runs of the same maneuver with both the full 20 mode and the reduced eight-mode models showed results that agreed closely).

The examination of these poles and zeros basically indicates that the structural modes that significantly affect the control design are those caused by the TDRSS antenna and the cryogen tank. (Since the pole-zero configuration is specific to the structural model and the axis analyzed, the previous statement is applicable only to the pitch axis of the FTM). The antenna's 1-Hz mode is uncomfortably close to the control system bandwidth of 0.48 Hz. Almost all the maneuvers simulated show significant excitation of this mode. The 18.94-Hz mode caused by the cryo tank required the design of a compensator by Bauer and Birky.

For this end-mounted spacecraft model, loop stabilization has been an important issue, both as mentioned by Bauer and Birky and as discussed above. The problem of stabilization is explained physically and the results obtained todate are elaborated.

RIG Loop Stabilization

A rather simplistic physical picture of the above system and of control-structure interaction can be drawn as follows: a sensor placed at a given point on the structure picks up the vibrations of the different modes at that point. If it is placed close to a node of a given mode, then it will scarcely be displaced by that vibration. Each complex pole-pair, or eigenvalue, represents one vibration. The gains are determined by the location of the actuator or sensor relative to the mode shape of a particular mode. The problem of stabilizing

the control system may be expressed in a nutshell by saying that the controller should provide negative feedback to each structural mode; at the very least, any positive feedback must be sizably below unit magnitude. If the structural damping coefficient for a given mode is very low, even a very small excitation of the mode will build up, if the controller pumps in energy in phase to the structural excitation. The total effect of the controller is essentially summarized in table 4. The first column shows the frequencies at which each mode resonates; because of the low damping, these are almost the natural frequencies of the structure. The second column has the modal gains at these frequencies. Note that the fourth modal gain is of the same order of magnitude as the first. The product of the controller gain and the modal gain is given in the fourth column. In this, the values for the higher modes are all much smaller than the first mode value. This is because this product does not account for the interaction between modes. A more elaborate computation that takes these effects into account gives the loop gain values in column 5 with the corresponding phase angles in column 6. The last column shows the real part or the inphase component of the modal excitation. All modes that show negative values in this column have positive feedback. Where the value is greater than unity in magnitude, the system behaves like a self-excited oscillator at that frequency. Any small excitation at that frequency comes back around the loop amplified and in phase and causes a buildup of oscillation. Thus the 21.2 Hz (133.2 rad/sec) mode is unstable while the 18.94 Hz (119 rad/sec) mode is close. Table 5 shows the effect of including the bending filter in the loop. The inphase components for the 18.94 and 21.2 Hz modes are reduced, the latter below unity and the system is stable.

Root-loci are drawn for the compensated system in figures 2-5. Figure 2 is an overall picture of the loci. Note the complex non-minimum phase zeros at $7.5 \pm 202i$. Almost symmetrically located in the left-half plane is another complex zero pair. There is a real zero in the right-half plane at 491. Another real zero is symmetrically placed at -490. A pair of complex zeros is located very close to the imaginary axis at $-0.02 \pm 43.5i$. The rigid body contributes an open-loop pole at the origin, while each mode appears as a complex pole-pair close to the imaginary axis.

The RIG contributes a complex pole-pair at $-12.6 \pm 21.77i$ (fig. 3). The bending filter (BF) zeros are placed close to the second bending mode, while its poles are about midway between the imaginary axis and the RIG poles (fig. 3). The PID controller and observer contribute two real poles at -0.06 and -0.07 and two zeros at -0.2 and -0.8 respectively.

From figure 4, the first bending mode is seen to be stabilized for all gains. One controller pole moves towards the adjacent controller zero. The other, together with the pole at the origin, gives a complex closed-loop pole-pair upto a gain of 1.5. The RIG poles move toward the BF zeros (fig. 3). The BF poles move toward the second mode zeros, while the second mode pole moves toward the zero at $43i$. This locus crosses the imaginary axis for a gain of 3. However, the system becomes unstable for a gain value of 1.5 as the locus from the 21.2 Hz (133.2 rad/sec) mode crosses the imaginary axis at this gain value (fig. 5).

Open-loop frequency response or Bode plots of this system are shown in figures 6 and 7. The system has a gain margin of 16.4 db at a crossover frequency of 1.94 Hz (12.19 rad/sec) and a phase margin of 54.2° with the corresponding crossover at 0.28 Hz (1.76 rad/sec). The closed-loop system bandwidth is 0.48 Hz (3 rad/sec).

Since the PID controller and observer are to be implemented digitally, it is important to check the loop stability of the resulting discrete system. This was done via the discrete root locus and all the closed-loop poles were found to lie within the unit circle in figure 8.

Next, the simulation results for the nod maneuver are discussed.

Simulation Results

The main difference between the earlier simulations and the current is that all the maneuvers are here commanded closed-loop. The observer and PID controller are kept in the loop throughout the maneuver. The maneuver command is initially a rate command, a triangle, a sine-versine or a ramp (for rasters). This forms a reference input to the RIG loop of the PCS (fig. 1). Subsequently, either a FGS output, or an artificially generated position error signal is used to correct for variations from the commanded attitude. This has the advantage that it is not dependant upon accurate knowledge of the moment of inertia value and obviates the need for an inertia estimator.

A triangle command input for a 450 arcsecond nod and a nominal slew time of 15 seconds is shown in figure 9. The peak rate commanded is 60 arcseconds/second. The attitude response at the FGS node is shown in figures 10 and 11. It is seen that the response settles to within 0.15 arcsec of the commanded attitude in 35 seconds. The RW torque time-history is shown in figure 12. The maximum torque is here limited to 1.5 Nm.

The effect of varying the nominal slew time, for a given maximum torque is shown in table 6. First, it is seen that there is a band of nominal slew times over which the response settles to the commanded value. At the lower end of this band, the torque demanded of the system is too high and the system response becomes oscillatory. (The response shows large swings in attitude with small damping). At the higher end, the torque profile is unsaturated and the full torque available is not being used. The response time obtained here is about the same as obtained open-loop in the earlier studies by Bauer and Birky and in reference 1. The variation of the commanded rate has about the same effect on the system as a variation in the moment of inertia (MOI). To check this out, the MOI was varied $\pm 25\%$ from the nominal value of 25330 kg. The maximum torque value was kept at 3.26 Nm (unpublished results, SIRTF Sensor and Actuator Detailed Design Definition Study, NASA Ames Research Center), while the FGS was switched on at $t = 10$, with $t_{slew} = 10$ seconds. The responses are shown in figures 13 and 14. (With the nominal MOI value, the settling time under the above conditions was 33 sec.) From figure 13, it is seen that lowering the MOI by 25% brings down the settling time to 20.5 sec. For the increased MOI, the settling time increases to 37 sec.

The main conclusion to be drawn from the aforementioned data is that if the system is designed with an upper bound on the MOI as the nominal value, it will give better responses at lower MOI values. With the maneuver being executed in a feedback fashion, it is unnecessary to change the command rate profile for up to a 25% change in the MOI for this single-axis model.

The reduction in the MOI above significantly improved the response. This suggests that an increase in the maximum torque capability should have the same effect. In a linear system with unbounded control capability, increasing the torque would have exactly the same effect as reducing the MOI (assuming that the bending modes are still damped out by the controller). However, in the nod maneuver investigations here, the phenomenon of saturation of the control effort complicates the issue. To avoid this problem and to speed up the response, the RWs are usually replaced by CMGs.

CMG SIMULATION RUNS

A SYSTEM_BUILD^{TM1} single-axis simulation of the PCS is shown in figure 15. All the component models are taken from Bauer and Birky. Here the RW-CMG combination is set up such that initially the CMG is used first and then control is switched to the RW. Although the CMG is switched off, it still outputs a sinusoidal mass unbalance torque of 5.4 Nm amplitude and a frequency of 100 Hz. The CMG has a resolution of 11 bits over its torque range. This effect is modeled by the quantizer in figure 15(d). The simulation also includes the effects of the CMG and RW torque ripples, figures 15(c) and (d), RIG drift and disturbance torques.

The maneuver was again commanded in a feedback fashion but with a sine-versine rate command as shown in figure 16. The first set of responses with CMGs alone is shown in figure 17. From figure 17(b), the settling time for the nod is seen to be 22.5 secs. There is an overshoot of 20% in the attitude at the RIG node (the attitude at the FGS node coincides with that at the RIG over this time interval). Figure 17(c) shows the residual oscillation at the FGS node; its amplitude is around 0.015 arcsec and the frequencies are about 2.2 and 19 Hz. The fundamental frequency for the RIG loop is about 1 Hz. The torque response (fig. 17(d)) displays large high-frequency content caused by the mass unbalance noise. This apparently does not affect the attitude response, essentially because it is a high-frequency jitter. The torque profile appears close to sine-versine despite the fact that the actual control effort is computed by the PID controller closed loop.

Switching in an ST reaction-wheel (0.3 Nm torque) 15 sec after the start of the maneuver only delayed the settling time to 23.5 sec; it did not reduce the amplitude of the residual oscillation. Delaying the switching to the RW till 25 sec after the start of the maneuver brought the settling time down to 22.5 sec.

The effects of torque disturbances and RIG drift on the system when controlled by CMGs were investigated. A steady disturbance torque of 0.05 Nm was introduced. This value is higher than the value employed in the Fairchild study (ref. 1). The external torque disturbances on the system arise from the gravity gradient, adiabatic demagnetization, solar radiation pressure, etc. These are all either constant or slowly varying compared to the maneuver duration. Thus, a constant disturbance level models their effect adequately. The RIG output was assumed to drift at a rate of 0.05 arcsec/sec. This models the effect of thermal bending on the pointing, where FGS correction is available. A settling time of 33 sec was obtained.

(**Author's note:** In the Fairchild study, the settling time for the nod maneuver was reported to be 6.5 sec, compared to the 22 sec figure obtained here. In their study, the maneuver was performed open loop, at least over the nominal slew time. However, since the control torque (fig. 17(d)), is close to sine-versine over the nominal slew time, the difference in the method of executing maneuvers should not be significant. This is being investigated further.)

The Effect of Increasing Torque

At this point, the following question arises: if the maximum torque is not a limiting factor on the performance, what is the lowest settling time that can be obtained for the given controller design (for the same gain values)? Note that even for a linear system (after removing both saturation and quantization effects), an analytical answer to this question would require the solution of two transcendental equations (one each for attitude and rate), so that settling time is not linearly related to the command profile.

[1] Trademark of Integrated Systems Inc., Santa Clara, CA.

The results of a simulation investigation of the previous question are shown in table 7. Here the FGS loop was switched in at the end of the nominal slew time. This is based on the argument that, at this time instant, the attitude angle would be close to the commanded value and the attitude rate would be small. The settling time is defined here as the total time required for the response to settle within 0.15 arcsec of the commanded attitude in absolute value. To clarify further, if $t = t_{set}$ is the settling time, θ_r, θ are the commanded and actual attitudes in arcsec respectively, then for all $t \geq t_{set}, |\theta - \theta_r| \leq 0.15$. (This is different from the definition in PD 1011; it is more restrictive in some ways, as will be seen later). From table 7, it is clear that there is no advantage in using sine-versine torquing for the nod maneuver. There is a nominal slew time for which the settling time is a minimum. The maximum torque required for this minimum is below that possible with the tilt table (4.745 Nm, from the SIRTF Actuator Study of Class and Welch). For lower slew times, the settling time increases because the rates generated are too high; for higher, the rates are too low and the attitude approaches the specified band too slowly. The sharp increase in the settling time between $t_{slew} = 9$ and $t_{slew} = 10$ is a consequence of the prior settling time definition as can be seen by comparing the corresponding responses in figure 18. Both responses reach $\theta = 449.85$ in the same time; however, the $t_{slew} = 10$ response leaves the 0.3 arcsec band over a short time interval and thus the settling time for it increases to 32 sec.

The definition of the settling time for the nod in PD 1011 is "the time required for structural vibration to settle to levels consistent with the specified stability." This may be interpreted as follows: the settling time t_{set}, is the first instant t such that

$$\left(\frac{1}{T}\int_{t_{set}}^{t_{set}+T}(\theta - \theta_r)^2\,dt\right)^{\frac{1}{2}} < 0.15.$$

Using this definition, the RMS error over $t \in [20, 30]$ was computed to be 0.116 for the $t_{slew} = 9$ case of table 7. This indicates a settling time below 20 sec for this response. The same computation for the $t_{slew} = 10$ case yields a 0.13 value. This is reasonable as can be seen from figure 18. In fact, if the maximum torque is limited to 3.26 Nm for the last run (which is the nominal situation), the RMS attitude error is 0.149 arcsec which is below the specification in PD 1011. **In this sense then, the nominal system with torque limited to 3.26 Nm does settle within 20 sec for a 450 arcsec nod.**

Finally, a nod response with a tilt table (torque limited to 4.745 Nm) is shown in figure 19, with all 20 structural modes included. The settling time (non PD 1011) is 20.8 sec and the RMS error over [20,30] is 0.116 arcsec.

The strategy of switching on the FGS loop exactly at the end of the nominal slew time is simple and seems to improve the system response. From figure 20, it is seen that postponing FGS switch to 15 sec for a nominal slew time of 9 sec, increases the settling time to 32 sec (non PD 1011 definition).

Next, the influence of FGS parameters on the system response are investigated.

FGS SIMULATION RUNS

The first FGS parameter of interest is the sampling time. All the results given so far, both here and in earlier reports assume a Fine Guidance Sensor sampling interval of 1 sec. The document PD 1011 states that "digital star location information will be provided with a frequency in the range of one every 0.2 to 10 sec." For the FGS system design, apparently longer sampling periods are much easier to achieve. With

this in mind, the FGS sample period was varied and the corresponding responses are tabulated in table 8. (The response for the 2 sec case is shown in fig. 21.) The table also shows the settling times as computed per the PD 1011 definition. The performance degradation for the 2 sec sampling period is marginal. For larger sampling periods, however, the response takes longer times to settle. Thus, it is possible to relax the FGS sampling requirement to once every 2 sec.

The resolution of the FGS is the next parameter of interest. The effect of this on the settling time and on the steady-state error was studied. A simulation interval of 60 sec was employed as the response was found to reach steady state within this interval. The results are shown in table 9. As may be expected, the steady-state error is the same as the resolution of the FGS; no other error sources are included in the simulation. The responses are plotted in figure 22. There is very little difference between the responses over the time interval [20,30]. The RMS error was computed over this time interval to determine the settling time and came below 0.15 arcsec for all three responses in the table. However, the times to settle within the 0.3 arcsec band varied considerably. This is essentially a consequence of fixing the averaging interval for the RMS error at 10 sec. The shaded areas in figure 22(b) cancel out giving an RMS error less than 0.15 arcsec. To confirm this effect, the averaging was carried out over the intervals [20,40] and [25,60] with RMS error results of 0.163 and 0.14 arcsec, respectively. This suggests two things: one, the RMS error based settling time for the third case of table 9 is around 25 sec and two, the definition of stability in PD 1011 should be changed to stipulate that the averaging of error be done until the response reaches steady state.

The noise from the FGS (or the noise equivalent angle) is another possible cause of degraded pointing performance. Since the FGS is yet to be designed, its noise characteristics are unknown. However, the simulation can be employed to investigate the effect of several possible noise levels. The noise distribution is assumed to be Gaussian with zero mean. Noise data generated for a standard deviation of 0.1 arcsec is shown in figure 23. The results are summarized in table 10. The response for the 0.1 arcsec case is shown in figure 24.

MODEL VARIATIONS

Control system designs make extensive use of the plant model (here the observatory model) when setting up the control law or algorithm. In practice, the model parameters are bound to vary. This variation can affect controller performance to various degrees; in the worst case it may even destabilize it. A controller design that is relatively unaffected by the variation of plant parameters over some specified ranges is said to be "**robust.**"

The main purpose of this subsection is to investigate how robust the PID controller for SIRTF actually is. A second aim is to determine what structural changes (if any), or changes in the location of sensors and actuators would help alleviate any robustness problems. The methods employed are first, stability analysis to determine if a parameter change destabilizes the system, second, simulation to compute nod response.

The first parameter of interest is the structural damping coefficient. In references 1 and 2, this is taken as 0.1% for all the modes. This is rather conservative for some modes as for those that are due to the TDRSS antenna, but not for the cryogen tank modes, for instance. Any further reduction in the damping coefficient for all the modes, say to 0.05% makes the system unstable (21.2-Hz mode). (Lowering the PID gains by 60% would make the system stable again, but would degrade performance).

Referring again to table 3, note that the significant modes at the lower frequency end are the TDRSS antenna modes. If the damping coefficients for these modes is increased to 1%, the individual modes are stabilized, but the overall system is not, as may be expected. The 21.2-Hz mode again crosses the imaginary axis for a multiplicative gain factor of 1.5. The settling time for the nod remains unchanged at 32 sec. Thus, simply increasing the TDRSS antenna damping alone, even by a factor of 10 will not improve performance. It is generally considered that increasing the cryogen tank damping coefficients would be difficult. However, the effect of having a 0.5% damping coefficient on the modes 3, 4, and 5 was to stabilize the 21.2 Hz mode for a gain up to 5 (the locus from the second bending mode still crosses the imaginary axis for a gain of 3). The settling time for the nod is 32 sec. In this case, however, the system nods and settles in 30 sec without the bending filter in the loop; or the bending filter is unnecessary. A further data point in this experiment of changing the structural damping coefficients was the increase of all coeff nts to 0.005. Here, too, the settling time without the filter was found to be 30 sec compared to 32 sec with it in the loop. These results are summarized in table 11.

Next the effects of variations in the modal frequencies are investigated. From table 3, the TDRSS antenna's first mode is only an octave off the control system bandwidth. Thus any further lowering of this modal frequency can be expected to adversely affect the system. When all modal frequencies were reduced by 25%, the system became unstable for $K_f = 0.6$ (compensated; 0.4 uncompensated). Several other combinations of frequencies were tried and were found to be unstable (cases 1-5 of table 12). Increasing all modal frequencies by 25% only degraded the performance slightly.

Increasing the structural damping so that all modes would have a damping coefficient of 0.005 essentially gives uniform performance over the $\pm 25\%$ modal frequency band (table 12). Here the bending filter is removed from the loop as it actually degrades the performance. Thus the main effect of increasing the structural damping would be to make the overall system more robust to modal frequency variations.

The gains corresponding to each structural mode depend primarily on the mode shape. Thus the easiest way to change these is to relocate the sensors and actuators, if other system considerations permit. This possibility is investigated next.

SENSOR-ACTUATOR PLACEMENT

From the flexible telescope model given by Bauer and Birky, modal gains are available at two actuator locations and two sensor locations; the effects of changing sensor and actuator positions on the structure can be studied by simply including different gain sets in the model. The underlying assumption is that the component being relocated does not significantly alter the mode gains.

The first case studied is where the RW is placed at the CMG location. All the original 20 modes were included in the root-locus shown in figure 25. The open-loop poles and zeros are given in table 13. Note the two pairs of complex nonminimum phase zeros in figure 25(a). The system remains stable upto $K_f = 3$ at which point the 3.58-Hz mode poles cross the imaginary axis (figs. 25(b) and (c)). The complex zero close to the imaginary axis for the baseline model has moved to higher frequencies (compare figs. 25(a) and (b) with figs. 2 and 3). The 18.94-Hz and 21.2-Hz modes hardly move with increase of the gain value (fig. 25(d)). A nod response with all 20 modes included but with no compensator is shown in figure 26(a), over the time interval [20,40] and in figure 26(b) over [40,60]. It has a settling time of 32.8-sec and an RMS error over [20,30] of 0.13. However, there is a residual 0.5-Hz oscillation of about 0.01 arcsec amplitude.

This configuration seems promising on account of the fact that the cryo tank modes no longer create a stability problem. It does require further study.

Next, the RWs are returned to their original location and the RIG is moved close to the FGS. For this configuration, the cryo tank modes at 18.94 and 21.2 Hz cause stability problems for the uncompensated system, even for $K_f = 0.5$. Including the bending filter in the loop does not help this problem.

The RWs are moved to the CMG node and the RIG is placed close to the FGS. The zeros and the open-loop poles are given in table 14. This time, the uncompensated system is stable upto a gain $K_f = 1.5$ when the 21.2-Hz mode crosses the imaginary axis. The corresponding root-loci are shown in figure 27. An extra complex zero pair appears in the left-half plane in figure 27(a). The zeros close to the imaginary axis in the baseline system disappear. The corresponding nod response over the interval [20,40] is shown in figure 28. The settling time (non PD 1011) is 32-sec and the RMS error over [20,30] is 0.142 arcsec. The response does not show the 0.5-Hz oscillation that occurs when the RW is alone relocated.

The effects of relocating the RW and RIG on the system behavior may be summarized as follows: moving only the RIG to the FGS position destabilizes the system; however, if the RW is simultaneously relocated to the CMG node, the uncompensated system is stable; it nods and settles in 32 sec (20.8 sec with tilt table). Relocating the RIG alone to the CMG node seems to give the most robust combination, except that the nod response shows a 0.01 arcsec amplitude oscillation at a frequency of 0.5 Hz.

In all of these simulations with reaction wheels, ideal wheels have been assumed and the noise from the RIG has been ignored. Torque quantization at the reaction wheel and the limit on RIG resolution are also neglected. In the next section, these effects are considered.

NOISE AND QUANTIZATION EFFECTS

A simulation model for the noise output of the RIG is given by Bauer and Birky. When this noise was included in the control loop with power spectral density as given in the reference, the effects on system performance were negligible. However, the DRIRU^{TM2} II literature also contains noise equivalent angle plots, like the one shown in figure 29. In an effort to incorporate this disturbance effect, and thermal bending in a somewhat worst-case sense, the noise equivalent angle profile shown in figure 30 was employed in the simulation. A 10-sec period was chosen for the slow variation of RIG output. In addition to noise, the RIG rate resolution was taken as 0.0125 arcsec/sec, again from Bauer and Birky.

The FGS was assumed to have a resolution of 0.01 arcsec and noise equivalent angle of 0.1 arcsec standard deviation. The reaction-wheel was modelled with mass unbalance and 11-bit torque quantization. The torque disturbance at the output of the reaction wheel was modelled in time as shown in figure 31.

The nod response with all these effects included is shown over the time interval [20,60] in figure 32, while the torque profile is shown in figure 33. The settling time (non PD1011) is 37 sec, essentially because of a small excursion of the response outside the 0.3 arcsec band around the commanded attitude. The RMS error over the time interval [20,30] is 0.17 arcsec, and over [30,40] it is 0.116 arcsec. Thus the effects of the disturbances are to increase the settling time for the nod (defined either as in PD 1011 or in absolute terms). On reversing the direction of the disturbance torque, the settling time remained at 37 sec, while the RMS error over the [20,30] interval was 0.155 arcsec.

[2] Trademark of Teledyne Systems, Northridge, CA.

If the maximum control torque available is increased to 4.745 Nm (tilt-table), the RMS error over the time interval [20,30] is now reduced to 0.136 arcsec. Again, as can be seen from figure 34, the increase in settling time is because of a marginal excursion out of the specified tolerance band.

In PD1011, a requirement for an Inertial Reference Unit pointing mode is stated where the telescope has to be pointed to within 0.5 arcsec of a specified target without FGS correction during the maneuver. The stability limit is specified as 0.15 arcsec. In the next section, such maneuvers are investigated.

MANEUVERS WITHOUT THE FGS

When the FGS is not available, the system has no sensor that gives attitude information at the focal plane. The RIG measures the change in attitude over a sampling period. This measurement is corrupted by noise and its precision is limited by the RIG 's resolution. If an FGS attitude reading is available at the start of the maneuver, the attitude during the maneuver is computed simply by summing the RIG measurements over the earlier sampling instants. (Eventually, this estimation of the attitude could possibly be improved by using more complicated filtering algorithms). In the current investigation, this attitude estimate replaces the FGS reading in the FGS loop and provides an attitude error signal. The maneuver is performed completely closed-loop as before with a triangle reference command.

Example nod responses are shown in figure 35. Here, the maximum torque is limited to 4.745 Nm with a nominal slew time of 9 sec. Torque disturbances are included but the RIG noise is excluded. The settling times are 16.7 sec for a 0.5 arcsec band and 46 sec to a 0.15 arcsec band. The RMS error over the time interval [20,30] is 0.26 arcsec, while that over the time interval [40,60] is 0.08 arcsec.

The specification document also stipulates that the observation period for this mode should be at least 900 sec. To test whether the system meets this requirement, a 900-sec run with RIG noise equivalent angle as shown in figure 30 was made. The last 100 sec of the response are shown in figure 36. It is seen that the system essentially follows the 0.1-Hz oscillation that is contained in the noise output by the RIG. Thus, if the peak-to-peak noise equivalent angle output of the RIG is within 0.06 arcsec over the 15-min observation period, then the telescope will be pointed within 0.5 arcsec of the commanded attitude over the observation period.

CONCLUSION

In this report, stability analysis and system simulation techniques have been employed to investigate the engineering issues delineated in the introduction. The results obtained are

a. Structural model effects: The modes due to the TDRSS antenna and the cryo tank significantly affect performance and stability. The 1.0-Hz mode of the antenna is only an octave above the control bandwidth. The cryo tank modes require the design of a bending compensator. The nominal system becomes unstable if the modal frequencies shift downward by 25%. If, however, the damping coefficients for all modes could be increased to 0.005, then the nominal system would yield uniform performance over $\pm 25\%$ modal frequency variation.

   If the RW is relocated to the CMG node and the RIG is moved close to the FGS, then the cryo tank modes do not destabilize the system. Bending compensation is unnecessary. The nod response settles in the same time as the baseline system. Relocation of the RW alone yields a stiffer system, but the

nod response shows a residual 0.5 Hz oscillation (0.02 arcsec, peak-peak). Moving the RIG alone to the FGS node destabilizes the system.

These configurations seem promising and will be explored further. Meanwhile, the physical meaning of this relocation needs to be clarified.

b. Fine Guidance Sensor Parameters: The effects of sampling period, resolution, and noise were investigated. A sampling period of 2 sec yields essentially the same performance as the baseline sampling period of 1 sec. Higher sampling periods severely degrade the nod performance. The precision achievable in pointing the telescope is directly related to the FGS resolution; thus a 0.1 arcsec resolution leads to a 0.1 arcsec steady-state error. (This is for a system that is ideal except for the finite FGS resolution). The noise equivalent angle of the FGS increases the settling time, the RMS error and the absolute error in the response. For a 0.15 arcsec RMS noise equivalent angle, the absolute error was found to be 0.07 arcsec.

c. Methods of maneuvering: Maneuvering closed-loop yields the same performance figures as feedforward torquing; it has the advantage that moment of inertia variation over $\pm 25\%$ does not increase pointing error. For the nod, a triangle rate command yields the quickest settling time of 20.8 seconds. This is for an ideal system with a maximum torque limit of 300 Nm. A nod can be performed using a tilt table (4.745 Nm maximum torque) in 20.8 sec. The use of CMGs does not reduce the settling time below this figure. The FGS loop should be switched on at the end of the nominal slew time selected.

   Maneuvering without the FGS is accomplished by computing attitude based upon the RIG and feeding a position error signal to the controller. For a small angle slew of 450 arcsec, settling to within 0.5 arcsec of the commanded attitude was achieved in 17 sec.

d. Disturbances: The disturbances modeled include RW and CMG mass unbalance; CMG torque ripple; external torque disturbances caused by ADR; gravity gradient and such; and FGS and RIG noise equivalent angle. With all disturbances included, a nod response with the tilt table took 37 sec. This deterioration, however, was due only to marginal excursions out of the ± 0.15 arcsec band around the commanded attitude (fig. 34(a)).

   A nod and 900-sec dwell was performed with gyros only and with all the above disturbance effects included and with RIG noise equivalent angle of 0.06 arcsec peak to peak. The telescope remained pointed within 0.5 arcsec of the commanded attitude over the entire observation period. The RIG noise equivalent angle was reproduced at the FGS node.

Redesign of the PID gains can improve the system response. Through parameter optimization of the PID gains it is possible to achieve a settling time of 21 sec with a 3.26 Nm maximum torque. This requires switching of the PID gains during the maneuver. These results will be described in a subsequent report.

REFERENCE

1. Class, B. F.; Bauer, F. H.; Strohbehn, K.; and Welch, R. V.: Space Infrared Telescope Facility/ Multimission Modular Spacecraft Attitude Control System Conceptual Design. *Annual AAS Guidance and Control Conference*, paper no. AAS 86-031, Keystone, CO, February 1–5, 1986.

TABLE 1.- CONTROLLER-OBSERVER-COMPENSATOR PARAMETERS FOR BASELINE SYSTEM

$K_P = 40000$ $K_R = 45009$ $K_I = 7710.5$

$K_1 = 0.1333$ $K_2 = 0.0044$

COMPENSATOR ZEROS AT -2.25+22.387i, -2.25-22.387i
COMPENSATOR POLES AT -6.6 +15.122i, -6.6 -15.122i
COMPENSATOR DC GAIN = 1.0

MOMENT OF INERTIA = 25330 KG M^2

TABLE 2.- INERTIAS IN THE SIRTF BODY COORDINATE FRAME

$I_{xx} = 10817$ $I_{xy} = 21.69$ $I_{xz} = -244.05$

$I_{yy} = 25327$ $I_{yz} = 17.626$

$I_{zz} = 23384$

ALL VALUES IN KG M^2

TABLE 3.- STRUCTURAL MODES IN SIMULATION MODEL

FREQUENCY (Hz)	DESCRIPTION
1.04	TDRSS ANTENNA (SPRING)
3.58	TDRSS ANTENNA (BOOM)
18.94	CT* YZ DISPLACEMENT
21.20	CT, OPTICS (X MMS) TORSION+MMS (SYM)
22.85	CT, OPTICS (X MMS) TORSION+MMS (ASYM)
30.18	MMS+VAC. HOUSING BENDING ABOUT Y MMS
32.26	MMS+VAC. HOUSING BENDING ABOUT X MMS
39.09	

*CRYOGEN TANK

TABLE 4.- MODAL RESONANCES AND THE UNCOMPENSATED CONTROLLER

Wm Rad/sec	Modal gain	Controller Gain	Product	Actual loop Gain	Phase Deg	Real Part Gain
6.5345D+00	3.3841D-05	4.5368D+04	1.5839D+00	1.0354D+01	-2.7790D+01	9.1594D+00
2.2494D+01	3.2017D-06	4.5039D+04	1.5479D-01	3.4825D+00	-9.0990D+01	-6.0196D-02
1.1900D+02	4.6607D-06	4.5010D+04	6.9264D-03	8.2462D-01	1.4972D+02	-7.1210D-01
1.3320D+02	1.0653D-05	4.5010D+04	1.1887D-02	1.5835D+00	1.4381D+02	-1.2780D+00
1.4357D+02	3.2020D-06	4.5010D+04	2.9441D-03	4.2361D-01	1.3767D+02	-3.1314D-01
1.8963D+02	-4.9556D-06	4.5009D+04	-2.1752D-03	4.1246D-01	-4.8700D+01	2.7223D-01
2.0270D+02	1.2960D-06	4.5009D+04	4.7432D-04	9.6067D-02	1.2923D+02	-6.0756D-02
2.4561D+02	-4.4029D-06	4.5009D+04	-9.4609D-04	2.3237D-01	-5.7185D+01	1.2593D-01

TABLE 5.- MODAL RESONANCES AND THE COMPENSATED CONTROLLER

Wm Rad/sec	Modal gain	Controller Gain	Product	Actual loop Gain	Phase Deg	Real Part Gain
6.5345D+00	3.3841D-05	4.6213D+04	1.5639D+00	1.0547D+01	-4.4812D+01	7.4821D+00
2.2494D+01	3.2017D-06	6.4882D+03	2.0773D-02	5.0169D-01	-1.2941D+01	-3.1850D-01
1.1900D+02	4.6607D-06	2.3665D+04	1.1030D-01	4.3355D-01	1.5387D+02	-3.8923D-01
1.3320D+02	1.0653D-05	2.3775D+04	2.5327D-01	8.3643D-01	1.4751D+02	-7.0553D-01
1.4357D+02	3.2020D-06	2.3836D+04	7.6320D-02	2.2434D-01	1.4109D+02	-1.7457D-01
1.8963D+02	-4.9556D-06	2.3994D+04	-1.1891D-01	2.1988D-01	-4.6124D+01	1.5240D-01
2.0270D+02	1.2960D-06	2.4021D+04	3.1130D-02	5.1270D-02	1.3164D+02	-3.4062D-02
2.4561D+02	-4.4029D-06	2.4080D+04	-1.0602D-01	1.2432D-01	-5.5210D+01	7.0930D-02

TABLE 6.- SETTLING TIME VERSUS NOMINAL SLEW TIME: NOD ANGLE = 450 arcsec, TORQUE BOUND = 1.5 Nm

TSLEW	SETTLING TIME
12	No settling
13	39.5
14	37
15	35
16	35 (max torque 1.4)
17	38.5 (torque unsaturated)
20	>40

TABLE 7.- SETTLING TIME VERSUS NOMINAL SLEW TIME FOR TRIANGLE AND SINE-VERSINE, FGS SWITCHED ON AT TIME = t_{slew}, NOD ANGLE = 450 arcsec, AND TORQUE BOUND = 300 Nm

TSLEW	SETTLING TIME (SAWTOOTH)	SETTLING TIME (SINE-VERSINE)
5		>40(31*)
6	>40 (10*)	22 (23.5*)
7	22.5(7.3*)	29 (17.5*)
8	21.2(5.6*)	34 (13.5*)
9	20.6(4.4*)	34.5(10.6*)
10	32 (3.6*)	35.4(8.1*)
15	34.6(1.6*)	37.5(3.3*)

*ACTUAL MAXIMUM TORQUE MAGNITUDE (NM)

TABLE 8.- SETTLING TIME VERSUS FGS SAMPLING PERIOD FOR 10-sec TRIANGLE NOD, FGS SWITCHED ON AT TIME = 10, NOD ANGLE = 450 arcsec, AND TORQUE BOUND = 3.26 Nm

TSF	SETTLING TIME	RMS ERROR*	SETTLING TIME(PD1011)
1	32	0.149	20
2	32	0.179	21
3	37	0.44	31
4	48	1.11	43
5	56	2.0	52

*COMPUTED OVER [20,30]

TABLE 9.- SETTLING TIME VERSUS FGS QUANTIZATION FOR 10-sec TRIANGLE NOD, FGS SWITCHED ON AT TIME = 10, NOD ANGLE = 450 arcsec, AND TORQUE BOUND = 3.26 Nm

RESO	SETTLING TIME	SETTLING TIME(PD1011)	STEADY-STATE ERROR*
0.01	32	20	0.01
0.05	34	20	0.05
0.1	40.5	20	0.104

*DEFINED AS ABSOLUTE ERROR AT T = 60 SEC

TABLE 10.- SETTLING TIME VERSUS FGS NOISE FOR 10-sec TRIANGLE NOD, FGS SWITCHED ON AT TIME = 10, NOD ANGLE = 450 arcsec, TORQUE BOUND = 3.26 Nm, AND FGS RESOLUTION = 0.01 arcsec

NEA	SETTLING TIME	RMS ERROR*	ABSOLUTE ERROR(T=60)
0	32	0.1	0.01
0.1	34.1	0.117	0.045
0.15	34.8	0.129	0.07

*COMPUTED OVER THE INTERVAL [20,60]

TABLE 11.- EFFECT OF MODAL DAMPING ON SYSTEM STABILITY AND PERFORMANCE

CASE	RESULTS
1)ALL 0.05%	UNSTABLE
2)1.04,3.58 1%	TSET=32, KF=1.5*, COMPENSATED
3)1.04,3.58 0.1%, 18.94-22.85 0.5%	TSET=30, KF=3*, UNCOMPENSATED
4)ALL 0.5%	TSET=30, KF=3*, UNCOMPENSATED
5)ALL 1%	TSET=30, KF=8*, UNCOMPENSATED

*KF MULTIPLIES THE PID GAINS TO GIVE ACTUAL GAINS

TABLE 12.- EFFECT OF MODAL FREQUENCY ON SYSTEM STABILITY AND PERFORMANCE

CASE	RESULTS
1)ALL 75%	UNSTABLE
2)1ST MODE 1.04 HZ, REST 75%	UNSTABLE
3)1ST&2ND MODES 1.04,3.58 REST 75%	UNSTABLE
4)MODES 3,4,5 SAME, REST 75%	UNSTABLE
5)MODES 1,3,4,5 SAME, REST 75%	UNSTABLE
6)ALL 125%	TSET=34.4 (RMS ERROR=0.147 OVER [20,30])
DAMPING COEFFICIENTS INCREASED TO 0.005	
1)ALL 75%	TSET=30.3 UNCOMPENSATED
2)ALL 125%	TSET=30.7 UNCOMPENSATED

TABLE 13.- OPEN-LOOP POLE ZERO PATTERN FOR RWA CMG SWITCH

POLES	ZEROS
0	
-6.0152D-02	-2.1875D-01
-7.3148D-02	-8.0323D-01
-2.9405D-03 +2.9405D+00i	-2.9405D-03 +2.9405D+00i
-2.9468D-03 +2.9468D+00i	-2.9265D-03 +2.9368D+00i
-3.5437D-03 +3.5437D+00i	-3.5437D-03 +3.5437D+00i
-3.5563D-03 +3.5563D+00i	-3.5563D-03 +3.5563D+00i
-6.2832D-03 +6.2832D+00i	-6.2832D-03 +6.2832D+00i
-6.5345D-03 +6.5345D+00i	-6.0922D-03 +6.3090D+00i
-7.9168D-03 +7.9168D+00i	-7.9168D-03 +7.9168D+00i
-1.6336D-02 +1.6336D+01i	-1.6336D-02 +1.6336D+01i
-2.2494D-02 +2.2494D+01i	-2.1138D-02 +2.1766D+01i
-1.2566D+01 +2.1766D+01i	
-1.1900D-01 +1.1900D+02i	-1.2477D-01 +1.2429D+02i
-1.2500D+02	
-1.3320D-01 +1.3320D+02i	-1.1842D+00 +1.3751D+02i
-1.3798D-01 +1.3798D+02i	9.0891D-01 +1.3751D+02i
-1.4357D-01 +1.4357D+02i	-1.4831D-01 +1.4800D+02i
-1.5972D-01 +1.5972D+02i	
-1.7775D-01 +1.7775D+02i	
-1.8963D-01 +1.8963D+02i	-1.0764D+01 +1.8237D+02i
-2.0270D-01 +2.0270D+02i	1.0400D+01 +1.8239D+02i
-2.3279D-01 +2.3279D+02i	-2.3165D-01 +2.3166D+02i
-2.3650D-01 +2.3650D+02i	-2.3786D-01 +2.3785D+02i
-2.4561D-01 +2.4561D+02i	
	1.4313D+02
	-1.4289D+02
	2.4815D+01 +1.9808D+02i
	-2.5215D+01 +1.9803D+02i

OF EACH COMPLEX CONJUGATE PAIR ONLY VALUE ABOVE REAL AXIS IS GIVEN

TABLE 14.- OPEN-LOOP POLE-ZERO PATTERN FOR RWA AT CMG NODE AND RIG AT FGS NODE

POLES	ZEROS
0	
-6.0152D-02	-2.1875D-01
-7.3148D-02	-8.0323D-01
-2.9405D-03 +2.9405D+00i	-2.9405D-03 +2.9405D+00i
-2.9468D-03 +2.9468D+00i	-2.9475D-03 +2.9471D+00i
-3.5437D-03 +3.5437D+00i	-3.5437D-03 +3.5437D+00i
-3.5563D-03 +3.5563D+00i	-3.5564D-03 +3.5563D+00i
-6.2832D-03 +6.2832D+00i	-6.2832D-03 +6.2832D+00i
-6.5345D-03 +6.5345D+00i	-6.5498D-03 +6.5423D+00i
-7.9168D-03 +7.9168D+00i	-7.9203D-03 +7.9186D+00i
-1.6336D-02 +1.6336D+01i	-1.6438D-02 +1.6394D+01i
-2.2494D-02 +2.2494D+01i	-2.2569D-02 +2.2540D+01i
-1.2566D+01 +2.1766D+01i	
-1.2500D+02	4.6218D+01
-1.1900D-01 +1.1900D+02i	-4.6174D+01
-1.3320D-01 +1.3320D+02i	-1.3550D-01 +1.3549D+02i
-1.3798D-01 +1.3798D+02i	-1.4065D-01 +1.4062D+02i
-1.4357D-01 +1.4357D+02i	-1.4591D-01 +1.4587D+02i
	-6.6699D+01 +1.8932D+02i
	6.6336D+01 +1.8947D+02i
-1.5972D-01 +1.5972D+02i	
-1.7775D-01 +1.7775D+02i	
	1.3124D+01 +1.9168D+02i
	-1.3508D+01 +1.9165D+02i
-1.8963D-01 +1.8963D+02i	-1.8507D-01 +1.8520D+02i
-2.0270D-01 +2.0270D+02i	
-2.3279D-01 +2.3279D+02i	
-2.3650D-01 +2.3650D+02i	-2.3503D-01 +2.3504D+02i
-2.4561D-01 +2.4561D+02i	-2.4561D-01 +2.4561D+02i

OF EACH COMPLEX CONJUGATE PAIR ONLY VALUE ABOVE REAL AXIS IS GIVEN

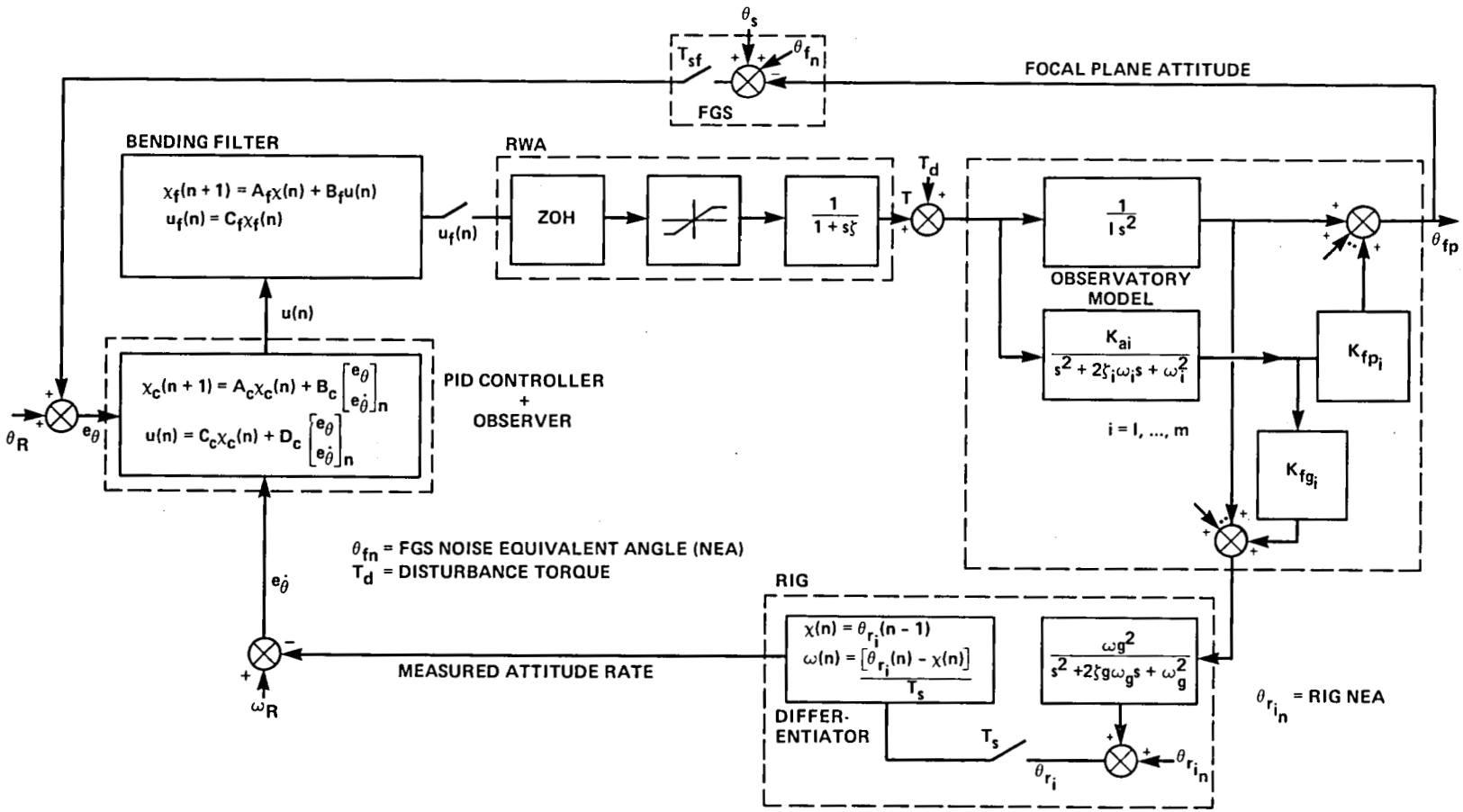

Figure 1.- Block diagram representation of the SIRTF attitude control system.

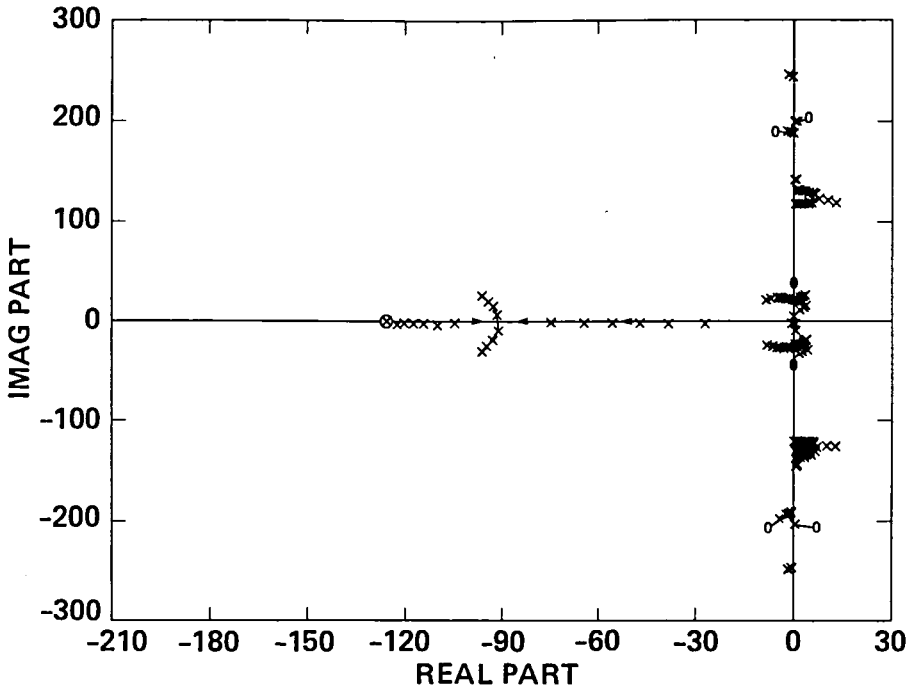

Figure 2.- Root locus of the SIRTF rate-integrating gyro loop showing structural modes up to 250 rad/sec.

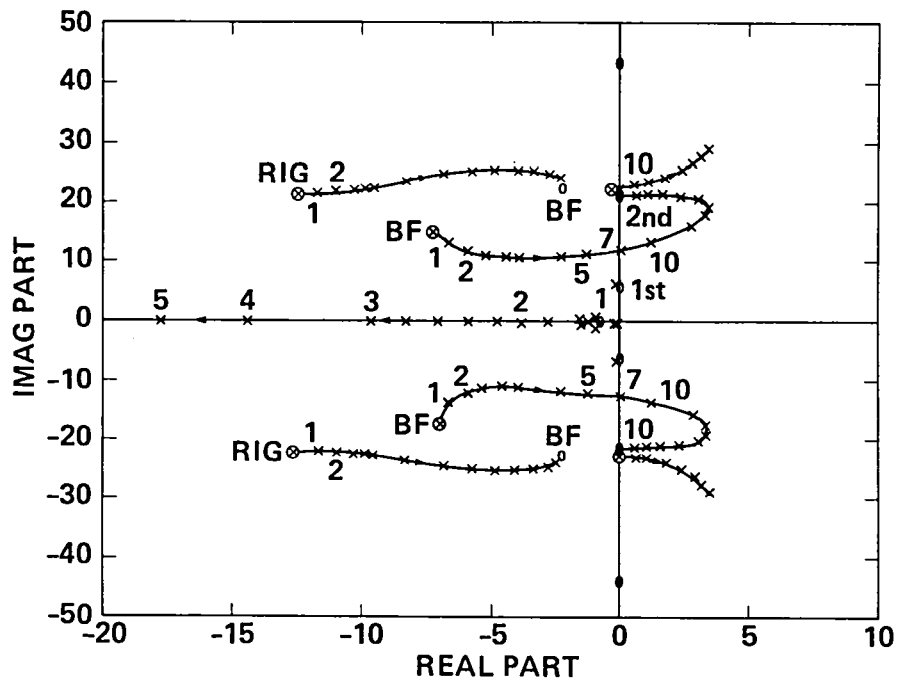

Figure 3.- Portion of root-locus showing the effects of rate-integrating gyro and the bending filter.

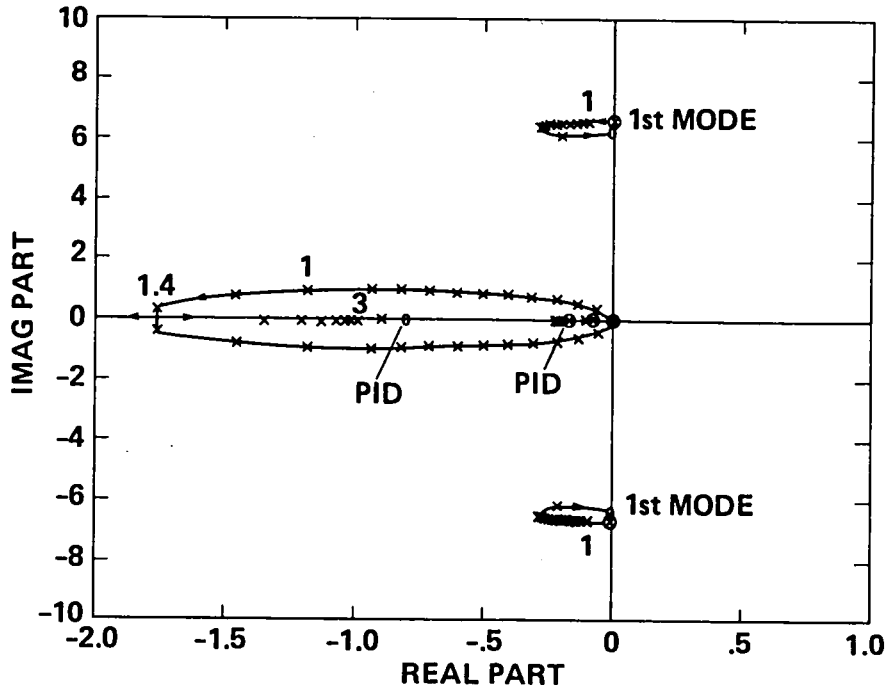

Figure 4.- Portion of root-locus showing the action of the PID controller.

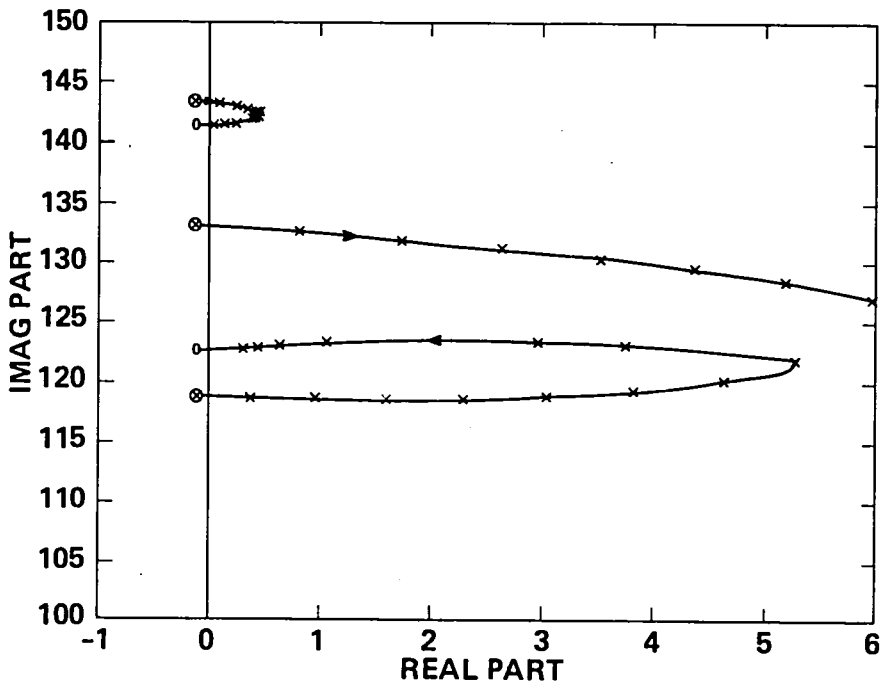

Figure 5.- Portion of the root-locus in the vicinity of the 133.2 rad/sec structural mode.

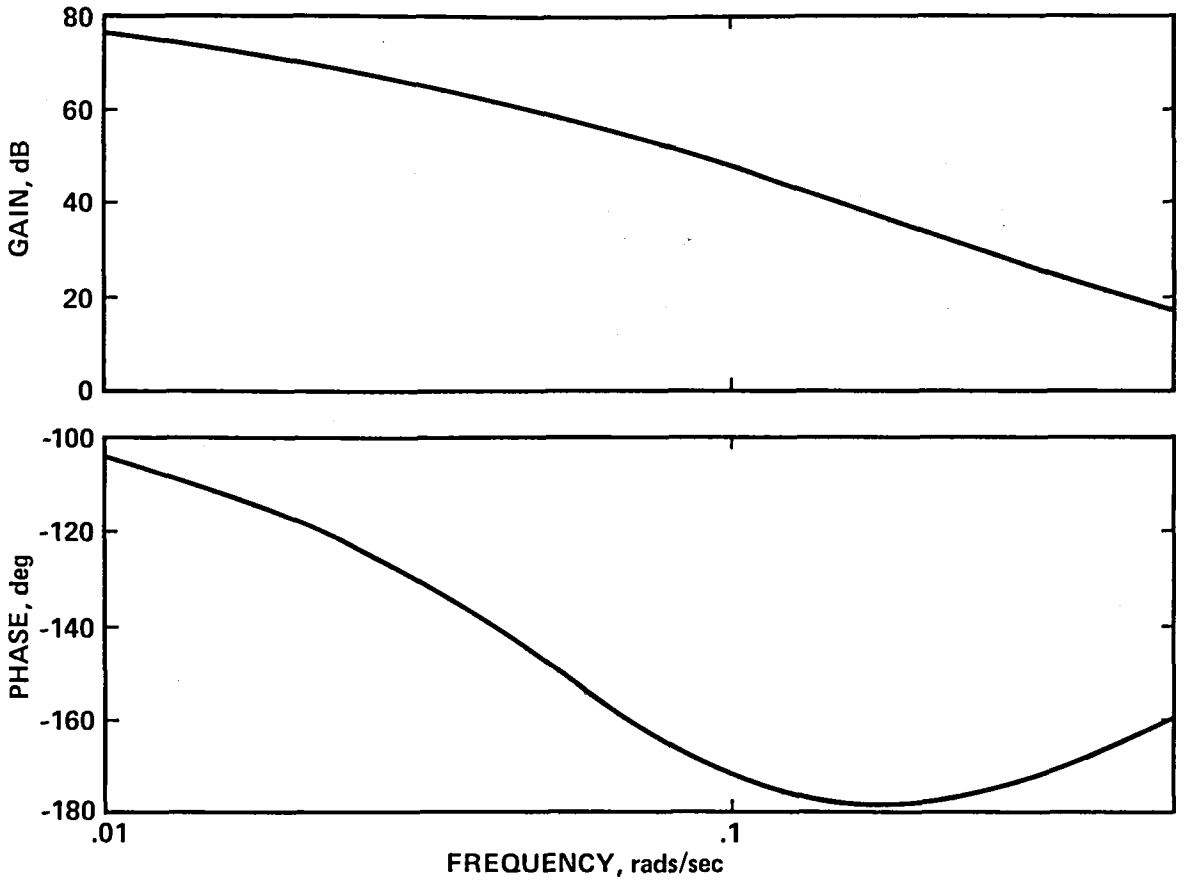

Figure 6.- Bode plot of the compensated rate-integrating gyro loop-frequencies up to 1 rad/sec.

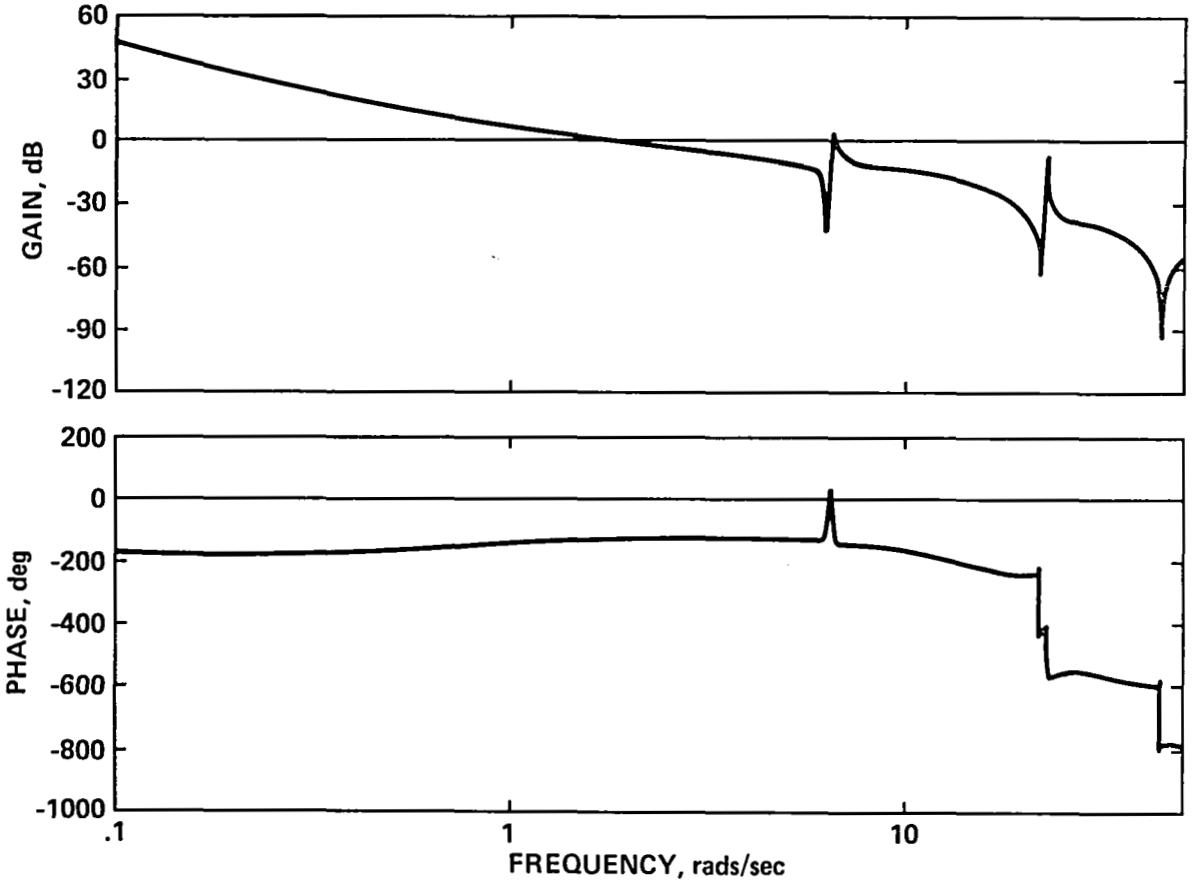

Figure 7.- Bode plot of the compensated rate-integrating gyro loop-frequencies up to 100 rad/sec.

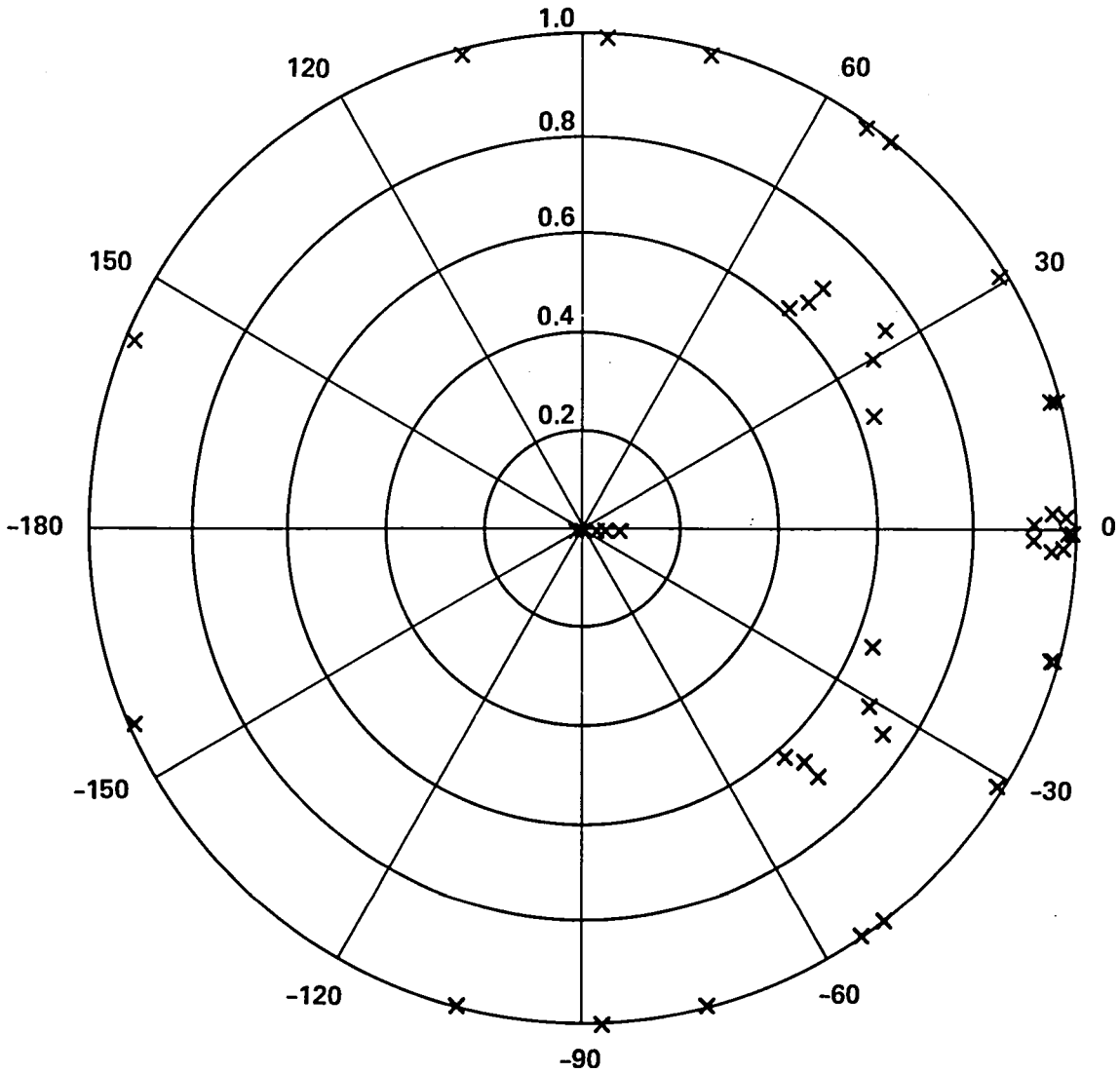

Figure 8.- Closed-loop eigenvalues of the discretized RIG loop; all lie within the unit circle in the z-plane.

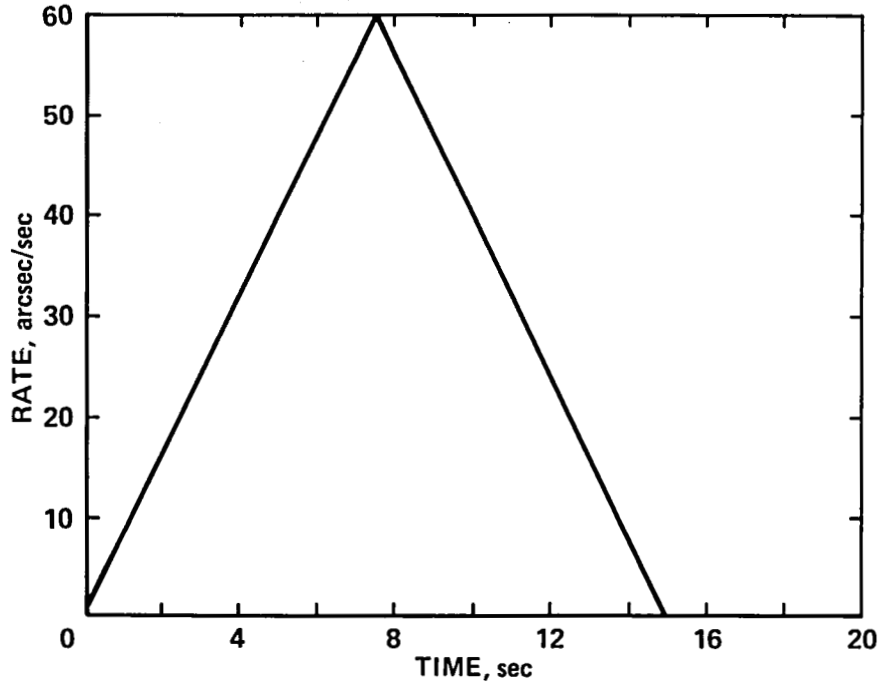

Figure 9.- A triangular rate command input to the attitude control system.

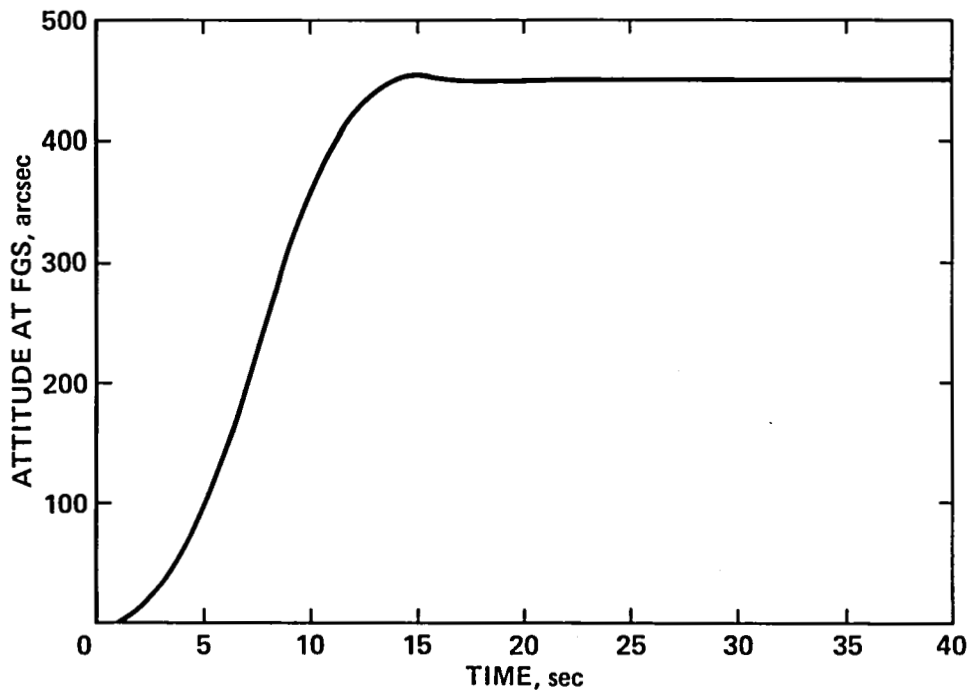

Figure 10.- Attitude response measured at the FGS node for a triangular rate command with nominal slew time = 15 sec.

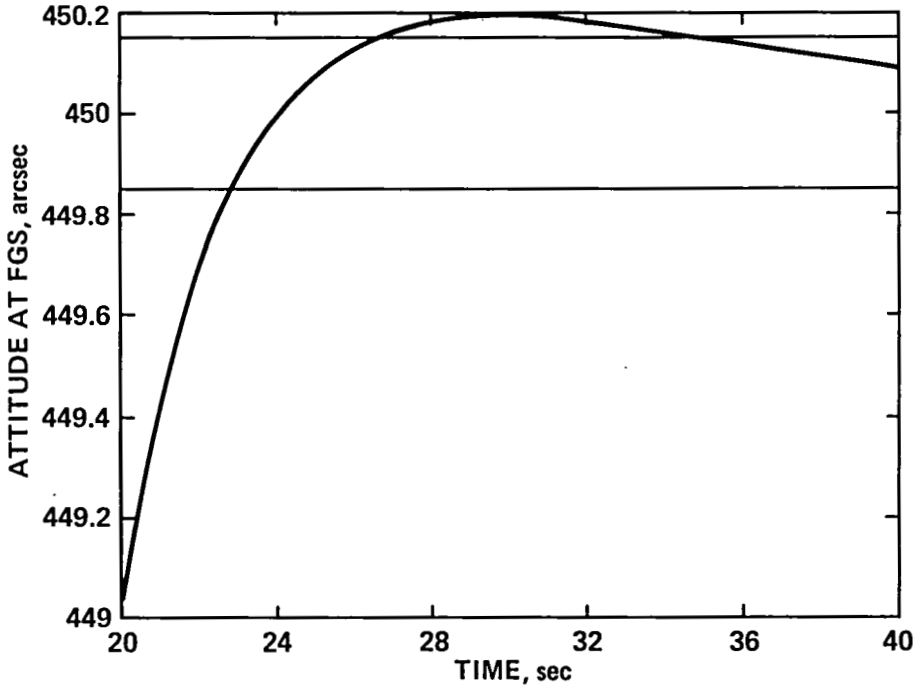

Figure 11.- Attitude response plotted over the time interval [20,40].

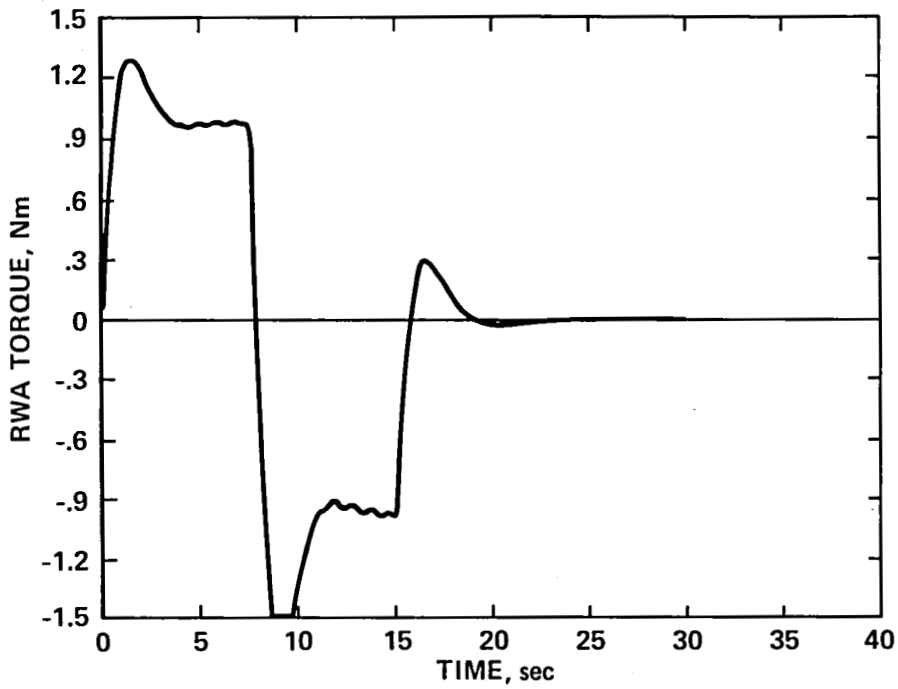

Figure 12.- Torque-time history for the maneuver shown in figures 10 and 11.

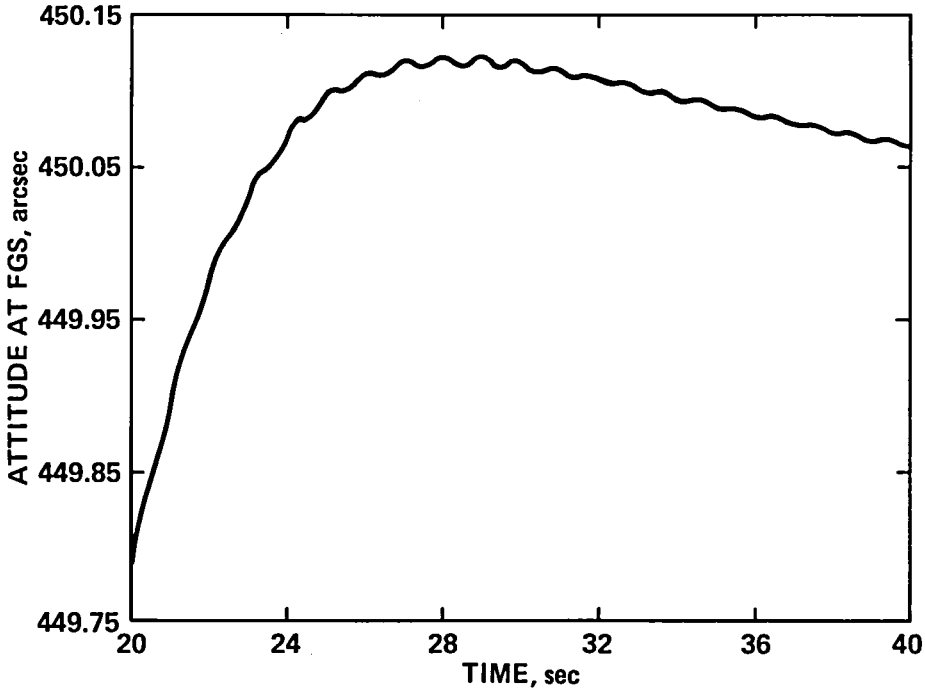

Figure 13.- Effect of reducing the observatory moment of inertia by 25% on the settling time.

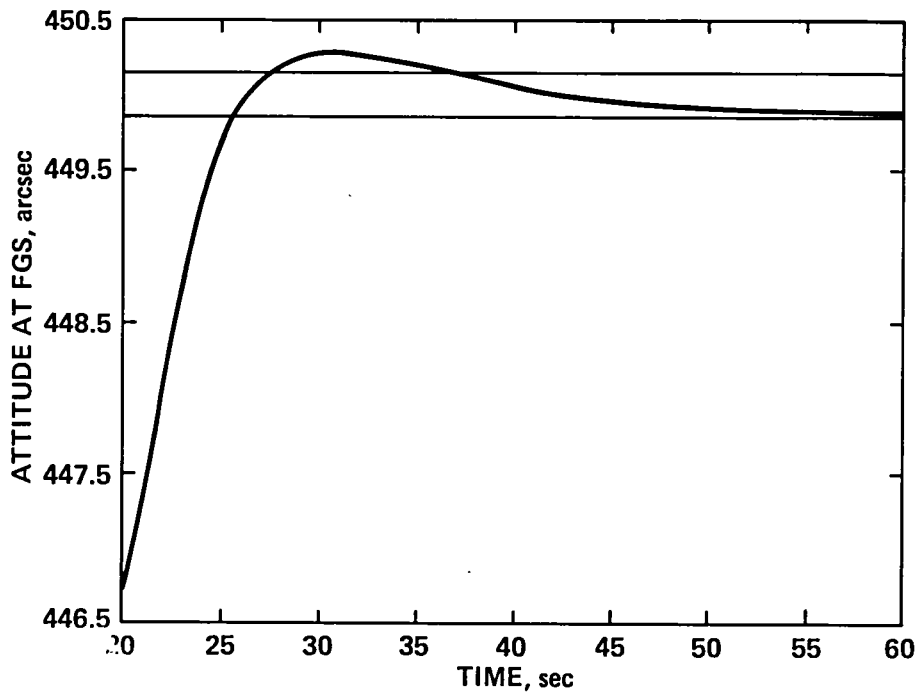

Figure 14.- Effect of increasing the observatory moment of inertia by 25% on the settling time.

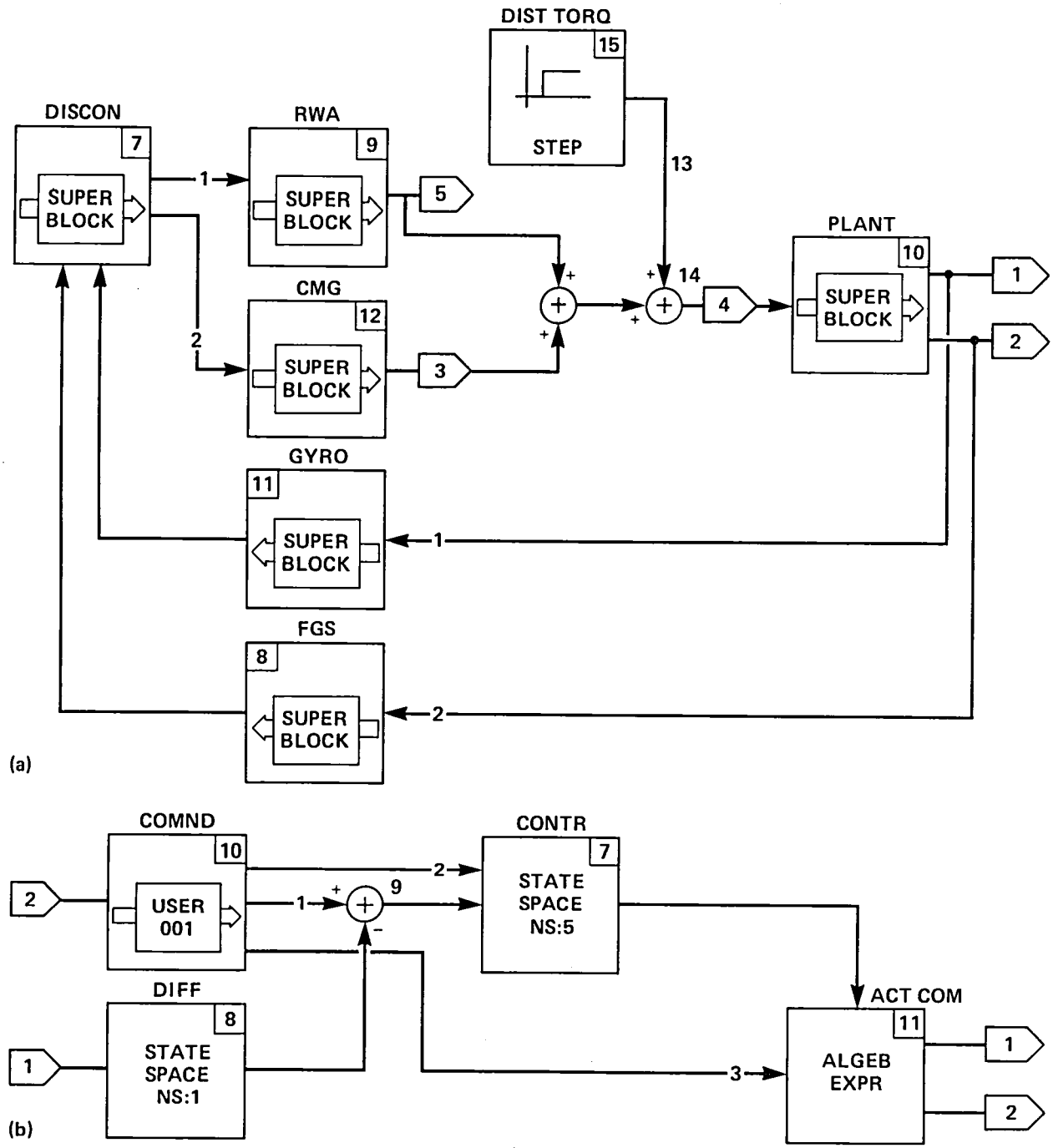

Figure 15.- A SYSTEM_BUILD^{TM} simulation of the overall attitude control system with reaction wheels and control moment gyros. (a) The complete system. (b) The discrete controller block "discon."

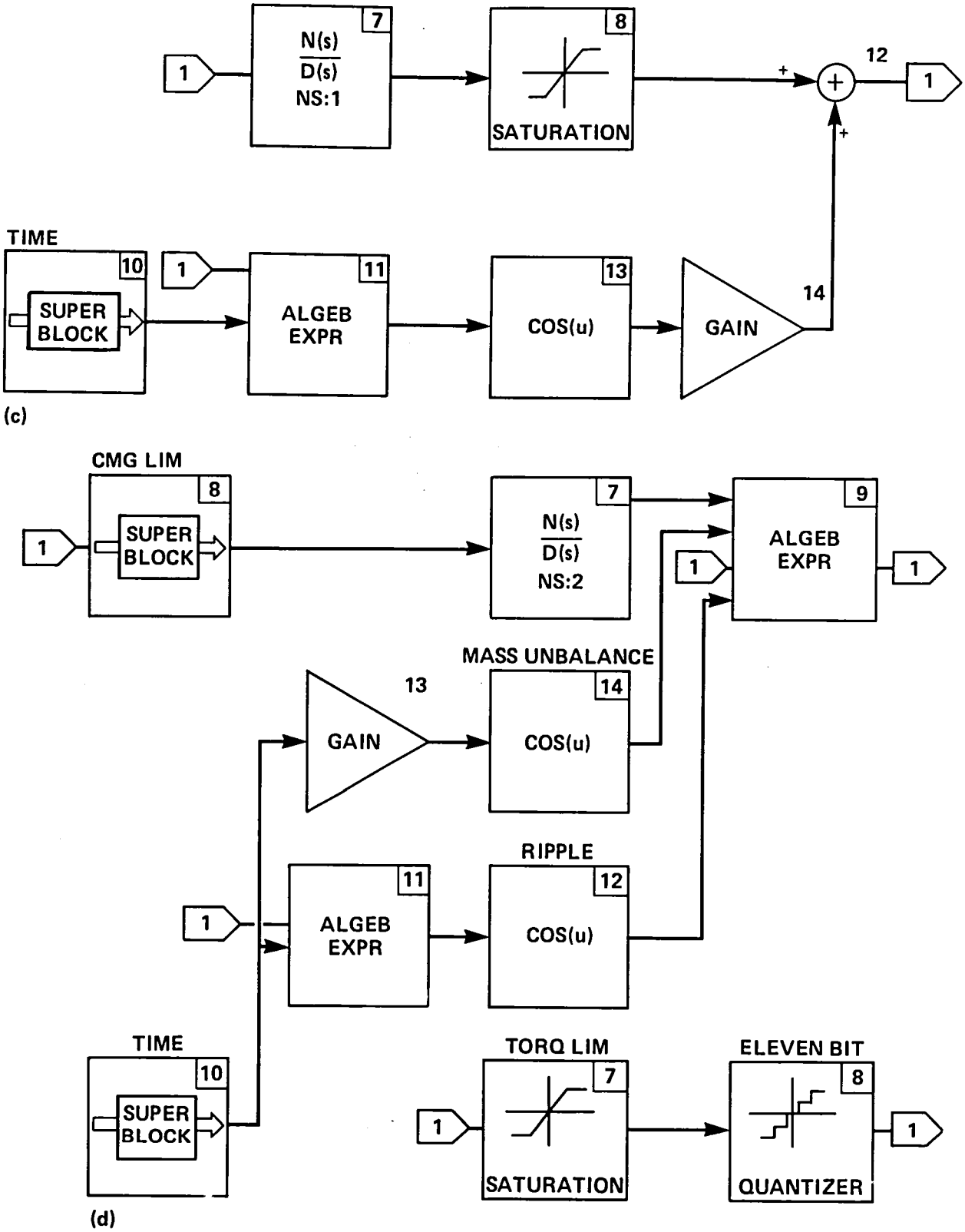

Figure 15.- Continued. (c) The continuous reaction-wheel block "rwa." (d) The continuous control moment gyro block "cmg."

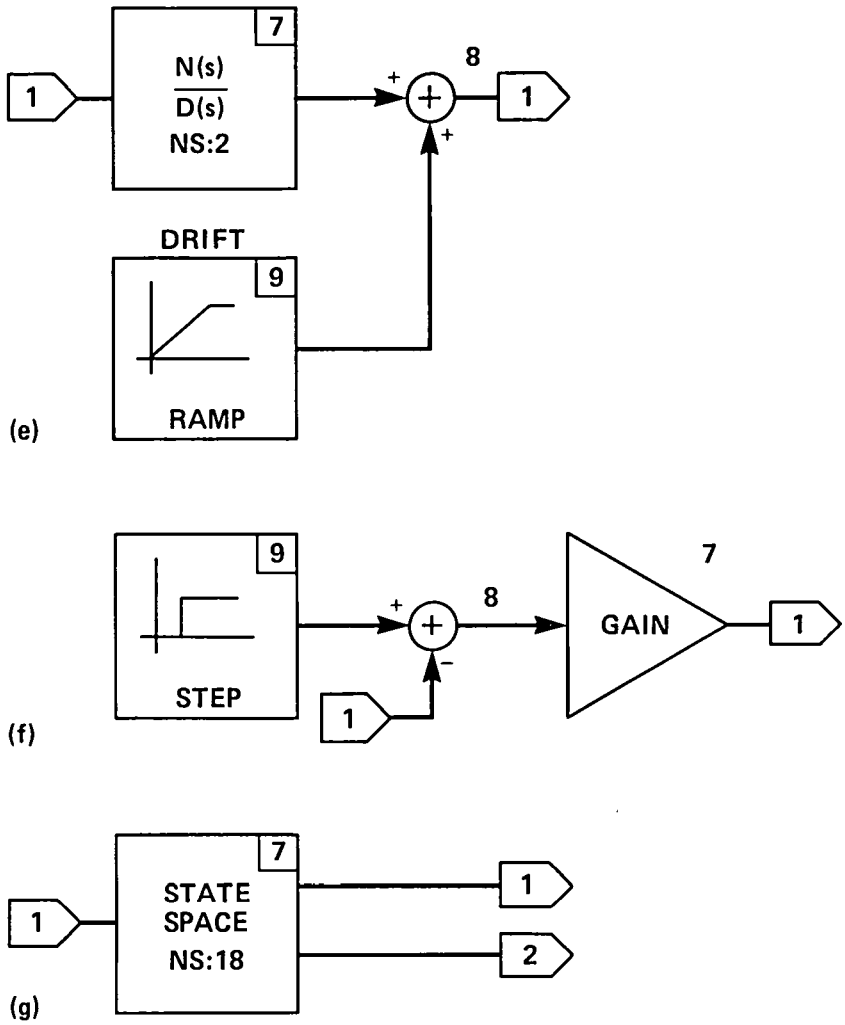

Figure 15.- Concluded. (e) The continuous gyro block "gyro" with drift included. (f) The discrete fine-guidance sensor block "fgs." (g) The continuous observatory dynamics block "plant."

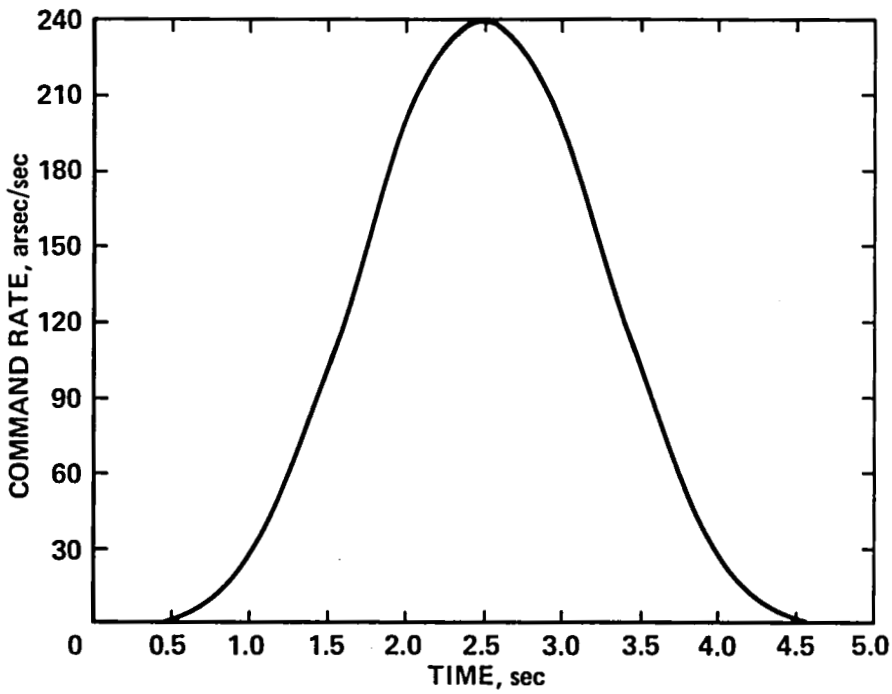

Figure 16.- A sine-versine rate command input to the attitude control system.

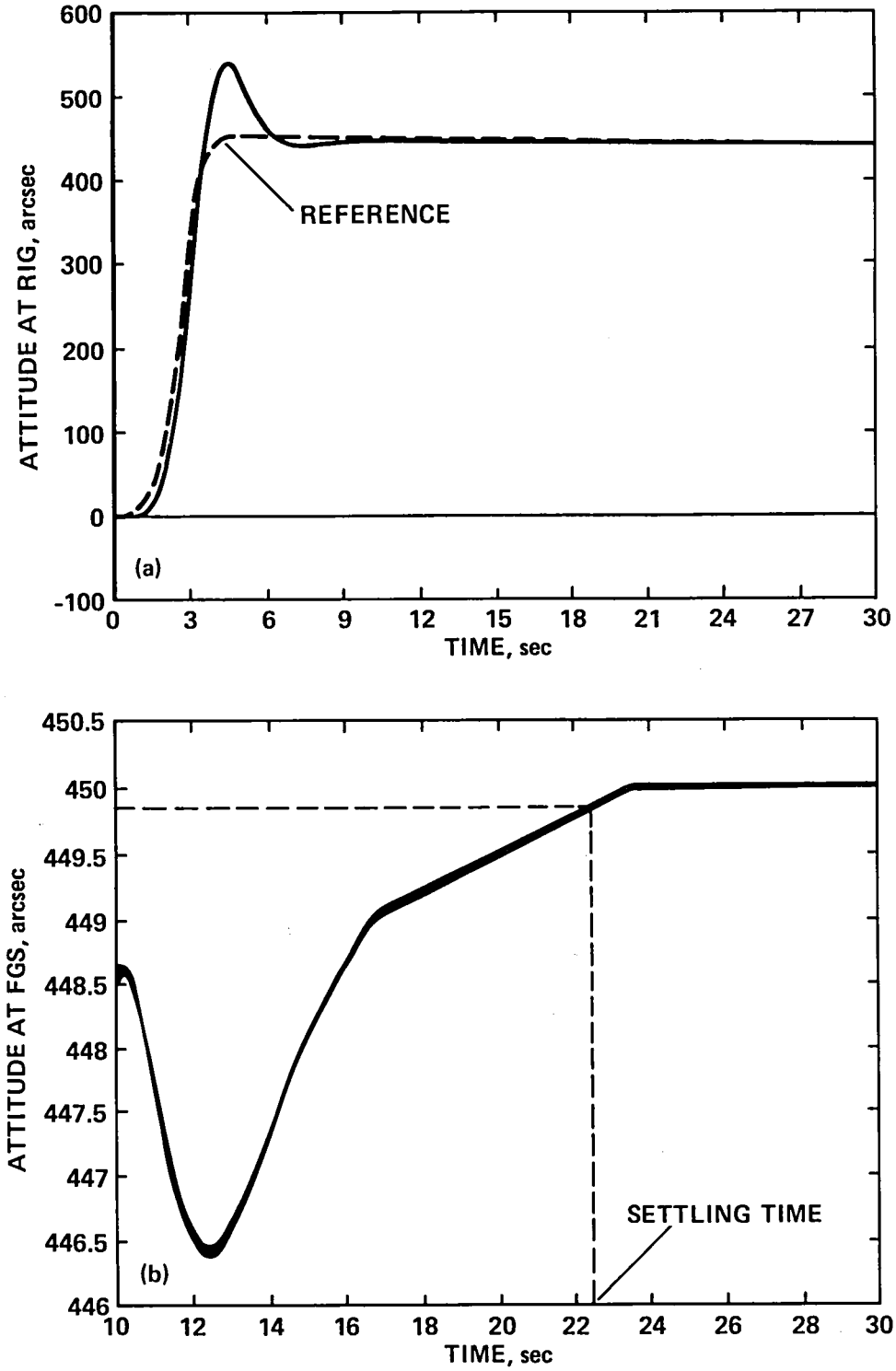

Figure 17.- Response time histories for a sine-versine rate command of 5-sec duration. (a) Attitude at the RIG node over the time interval [0,30]. (b) Attitude at the FGS node over the time interval [10,30].

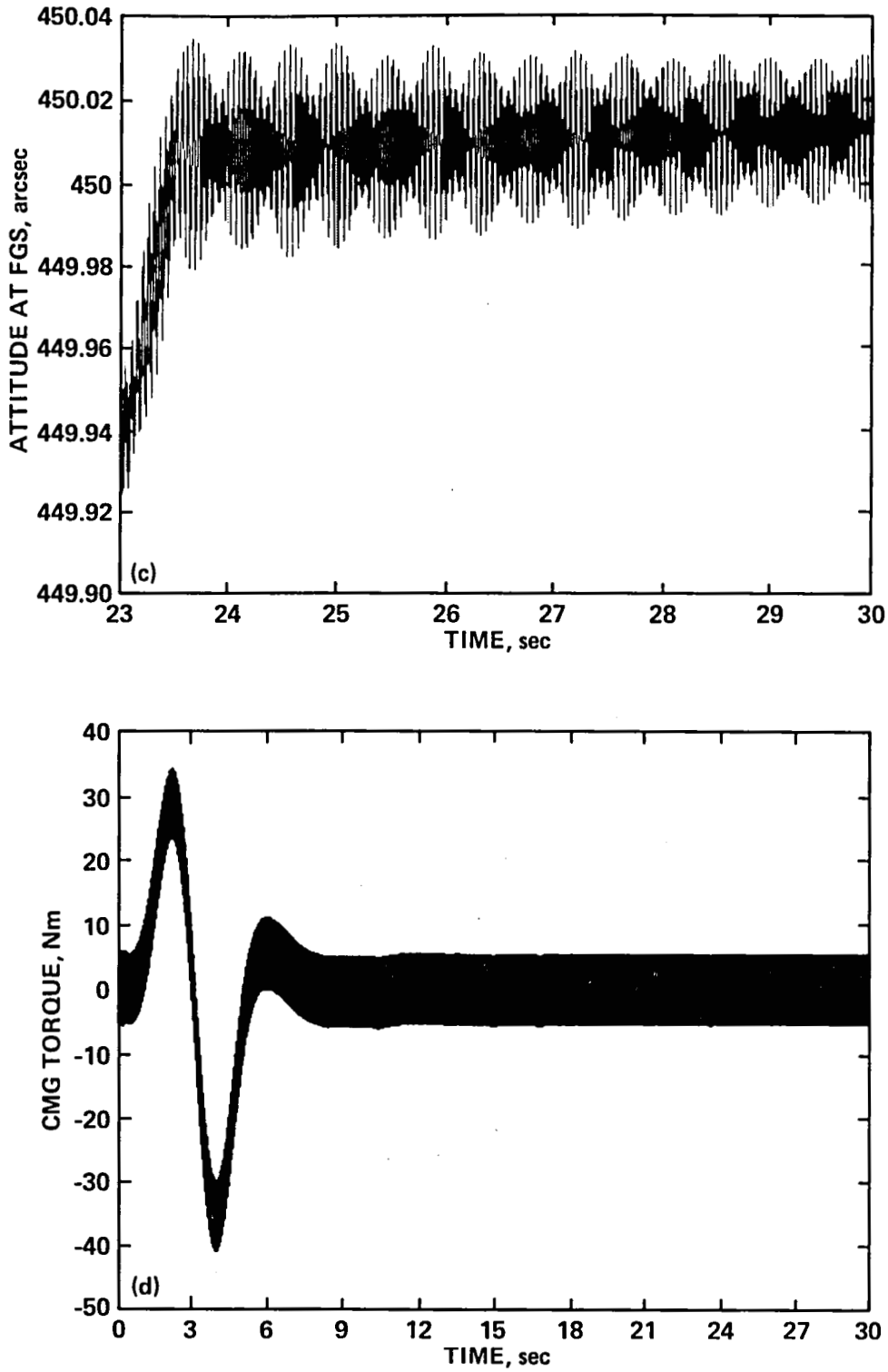

Figure 17.- Continued. (c) Attitude at the FGS node, magnified to show the effect of torque ripple. (d) The CMG torque time history.

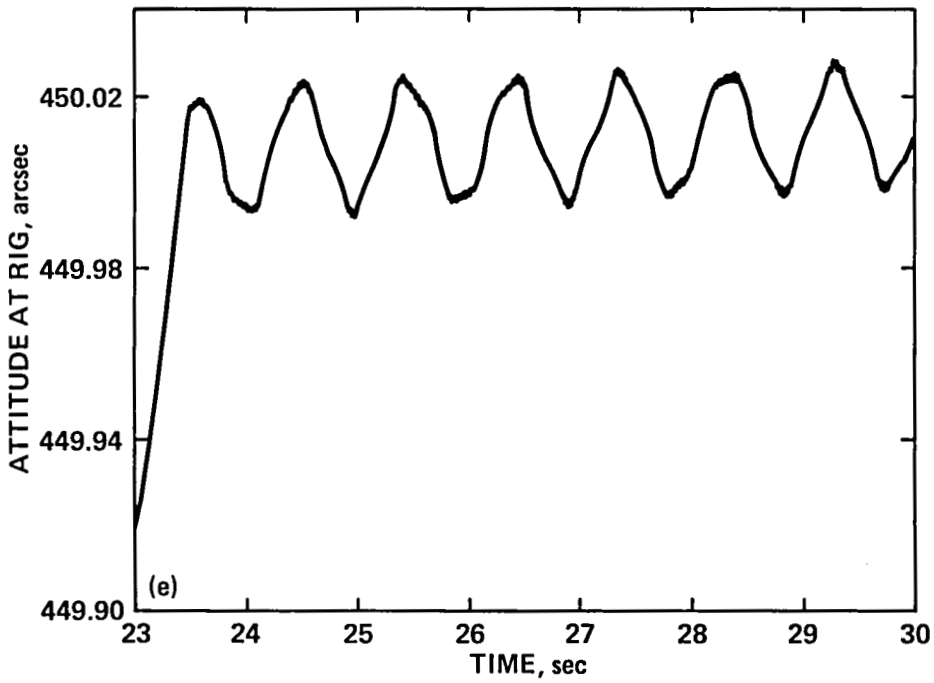

Figure 17.- Concluded. (e) Attitude at RIG magnified to show residual oscillation.

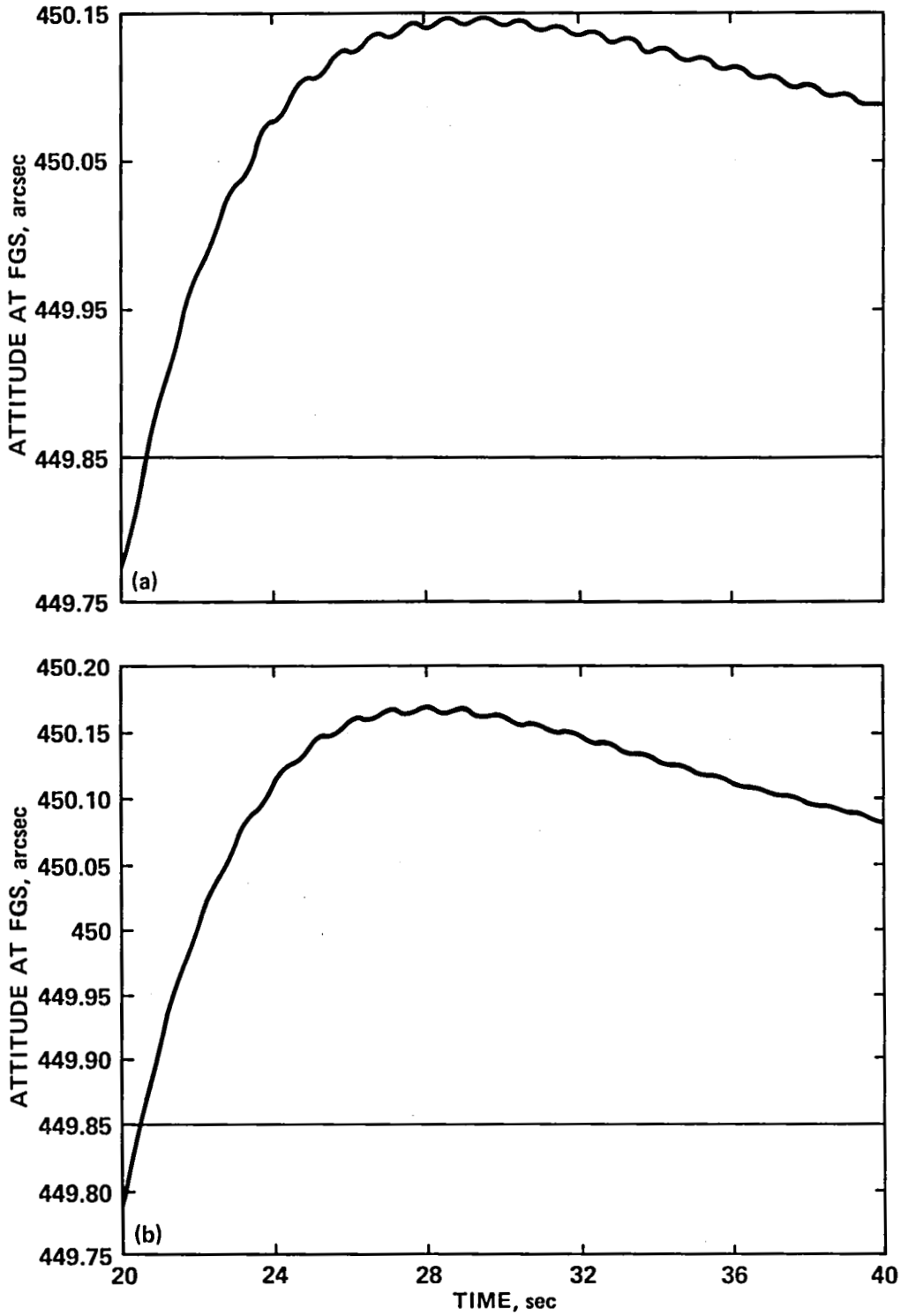

Figure 18.- Attitude response at the FGS node to a triangular rate command of 9-sec duration with maximum torque = 300 Nm, over the time interval [20,40]. (a) The FGS switched on 9 sec after start of maneuver. (b) The FGS switched on 10 sec after start of maneuver.

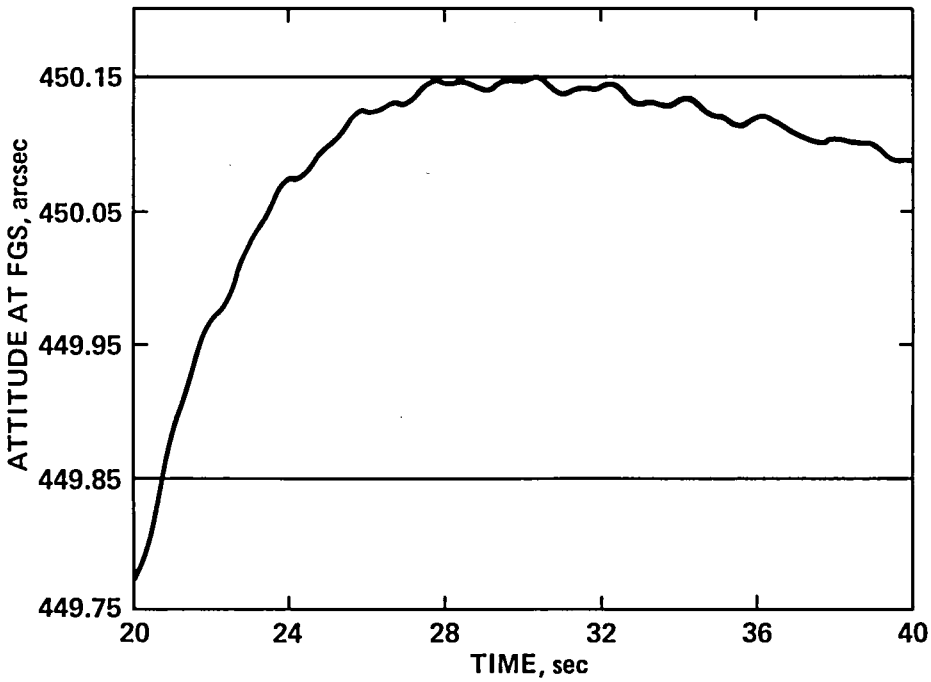

Figure 19.- Attitude response to a triangular rate command of 9-sec duration with a tilt-table actuator arrangement and 20 bending modes included in the observatory model.

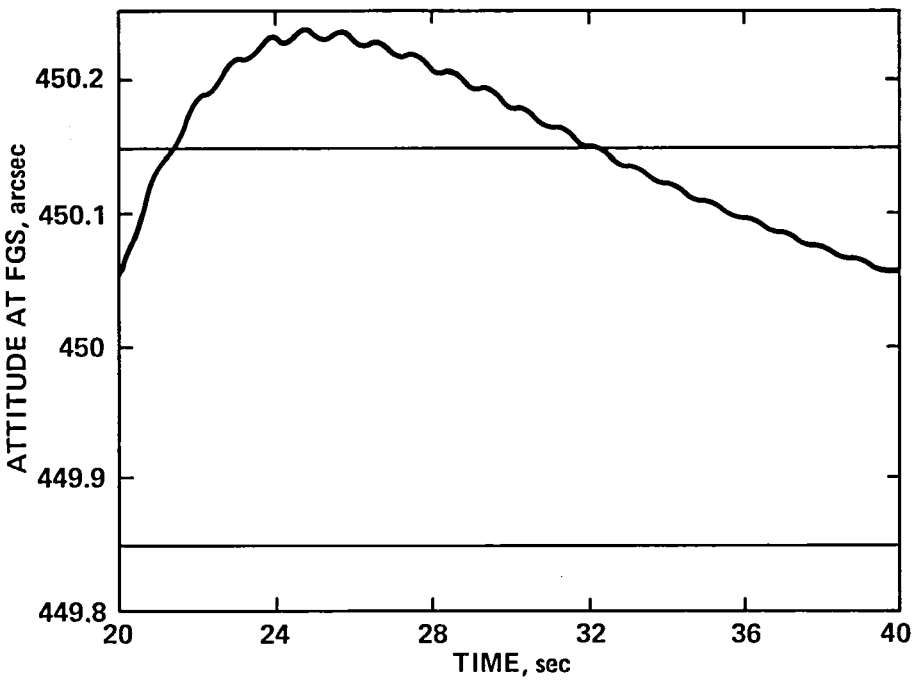

Figure 20.- Switching on the FGS 15 sec into the maneuver delays settling.

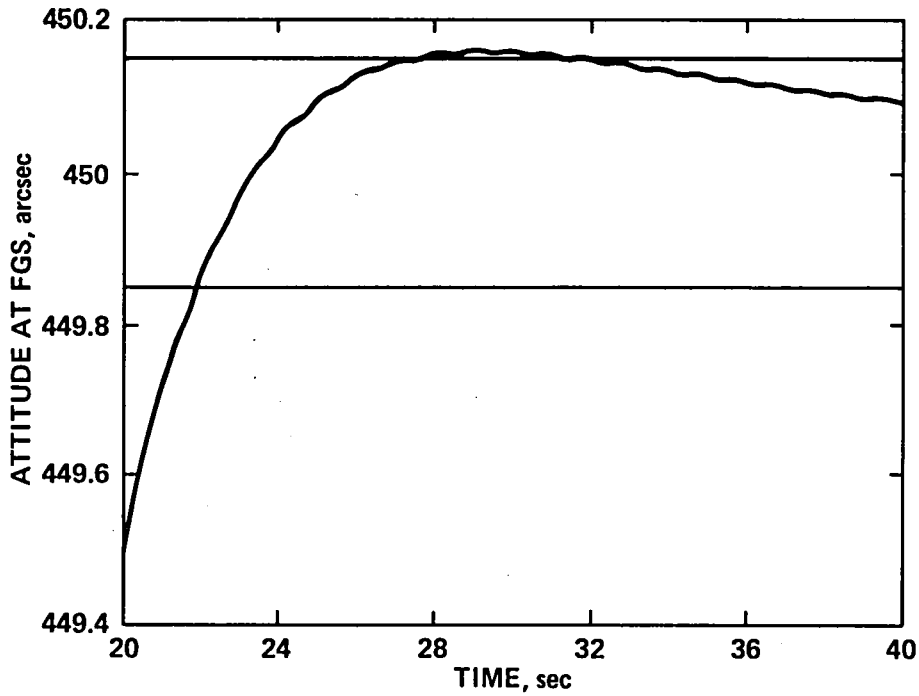

Figure 21.- Attitude response to a 10-sec duration triangular rate command, with FGS sample period of 2 sec and maximum torque limited to 3.26 Nm.

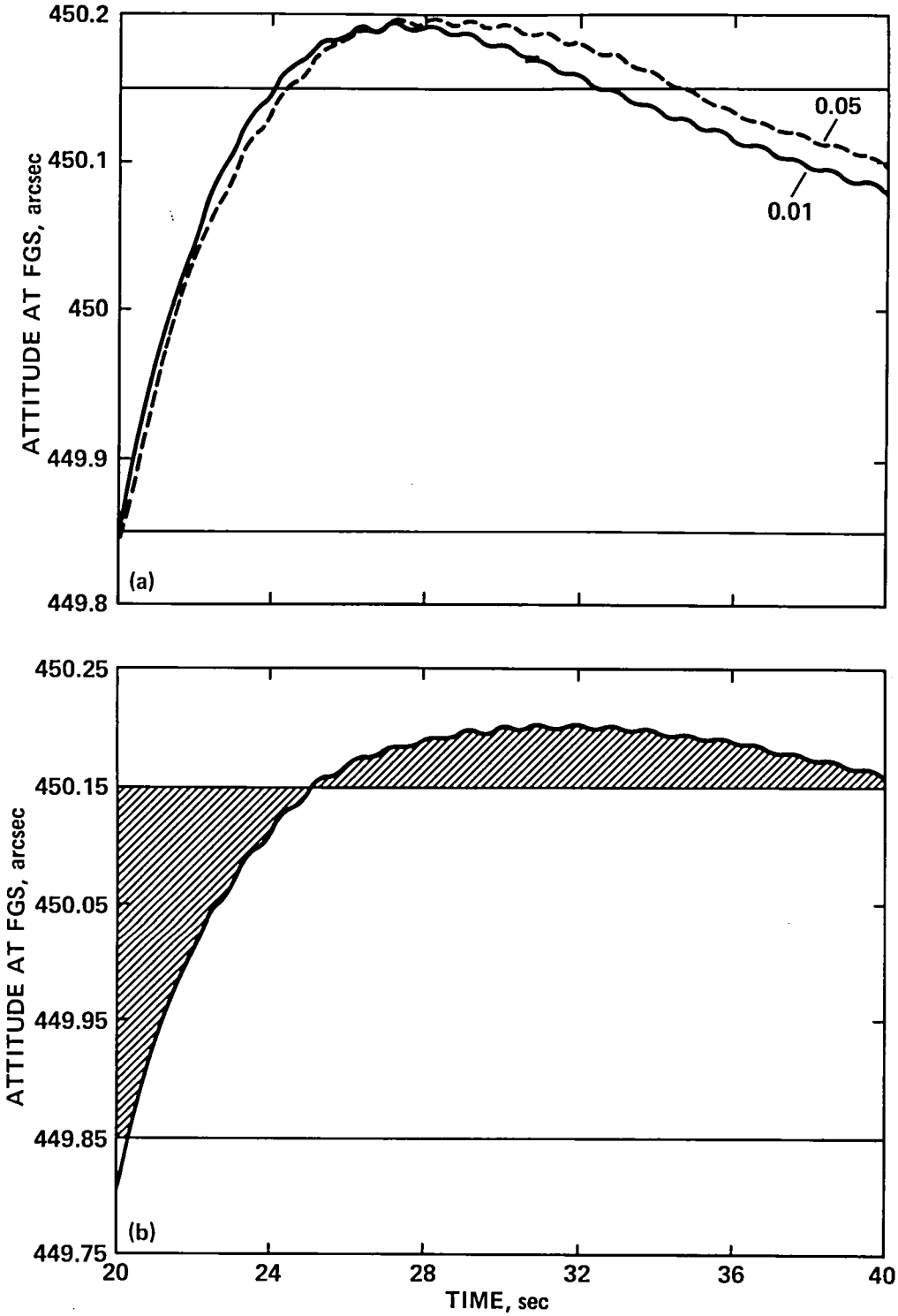

Figure 22.- The effect of finite FGS resolution upon the attitude response. (a) A quantization level of 0.01 arcsec. (b) A quantization level of 0.1 arcsec.

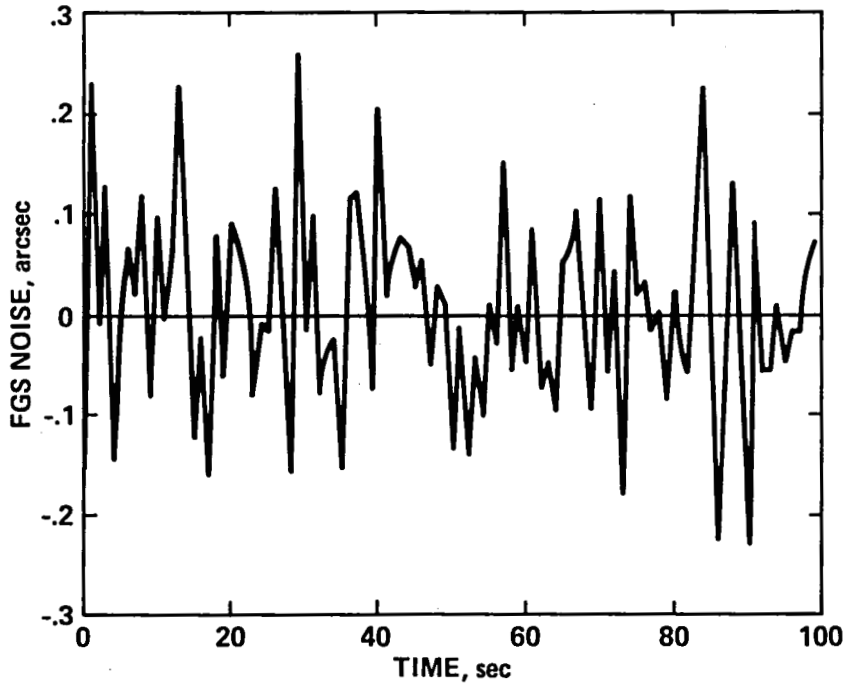

Figure 23.- The FGS noise-equivalent angle profile with 0.1 arcsec standard deviation.

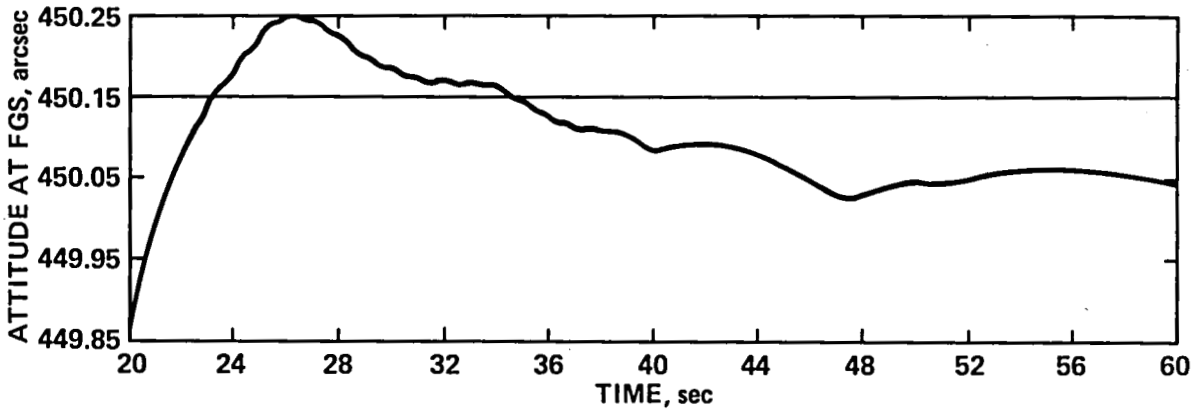

Figure 24.- Attitude response to a triangular rate command of 10-sec duration with FGS noise included in the simulation.

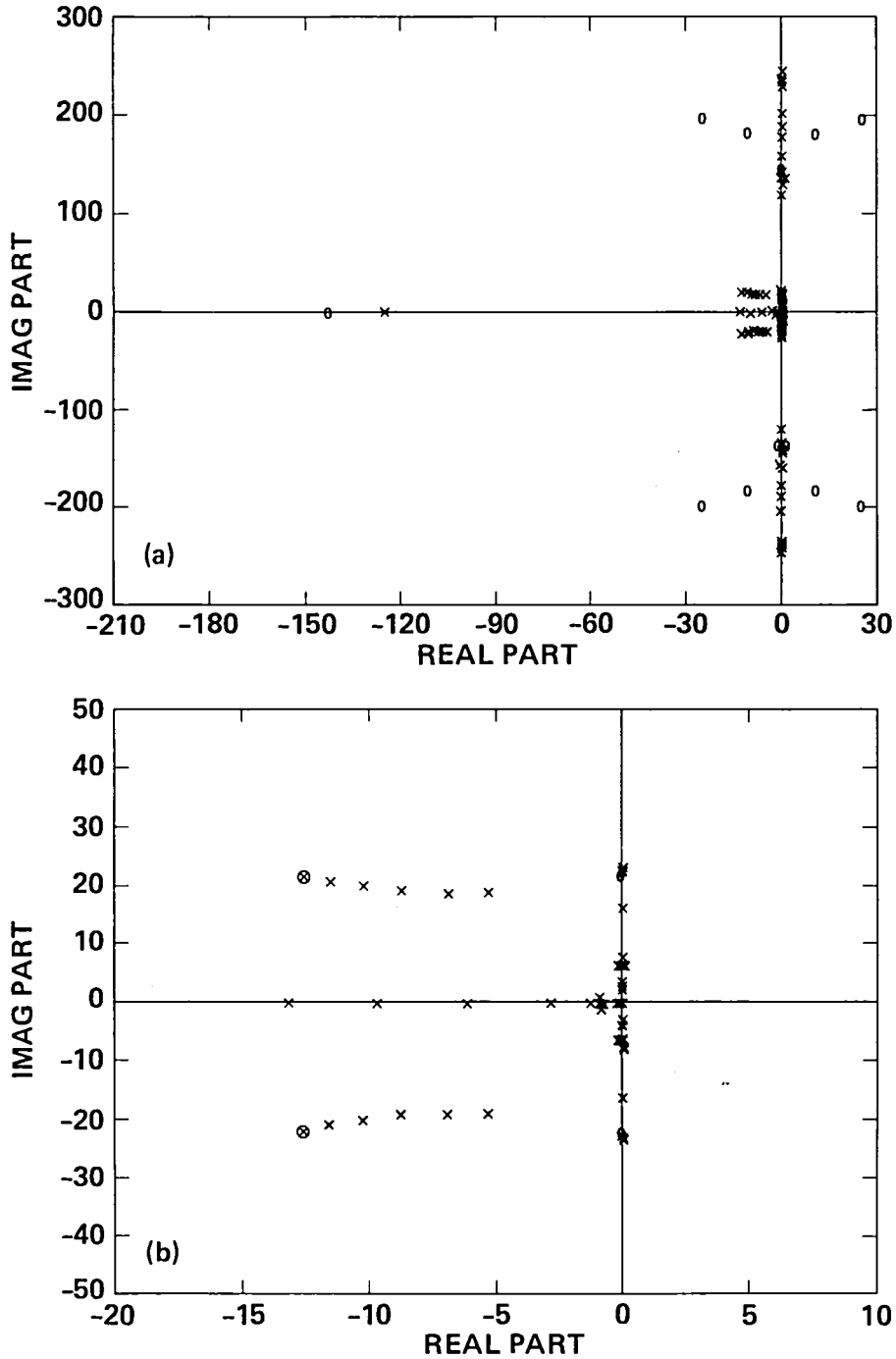

Figure 25.- Root-locus of the RIG loop with the reaction wheel located at the CMG node (all 20 bending modes included). (a) Overall picture including all modes. (b) In the vicinity of the RIG poles.

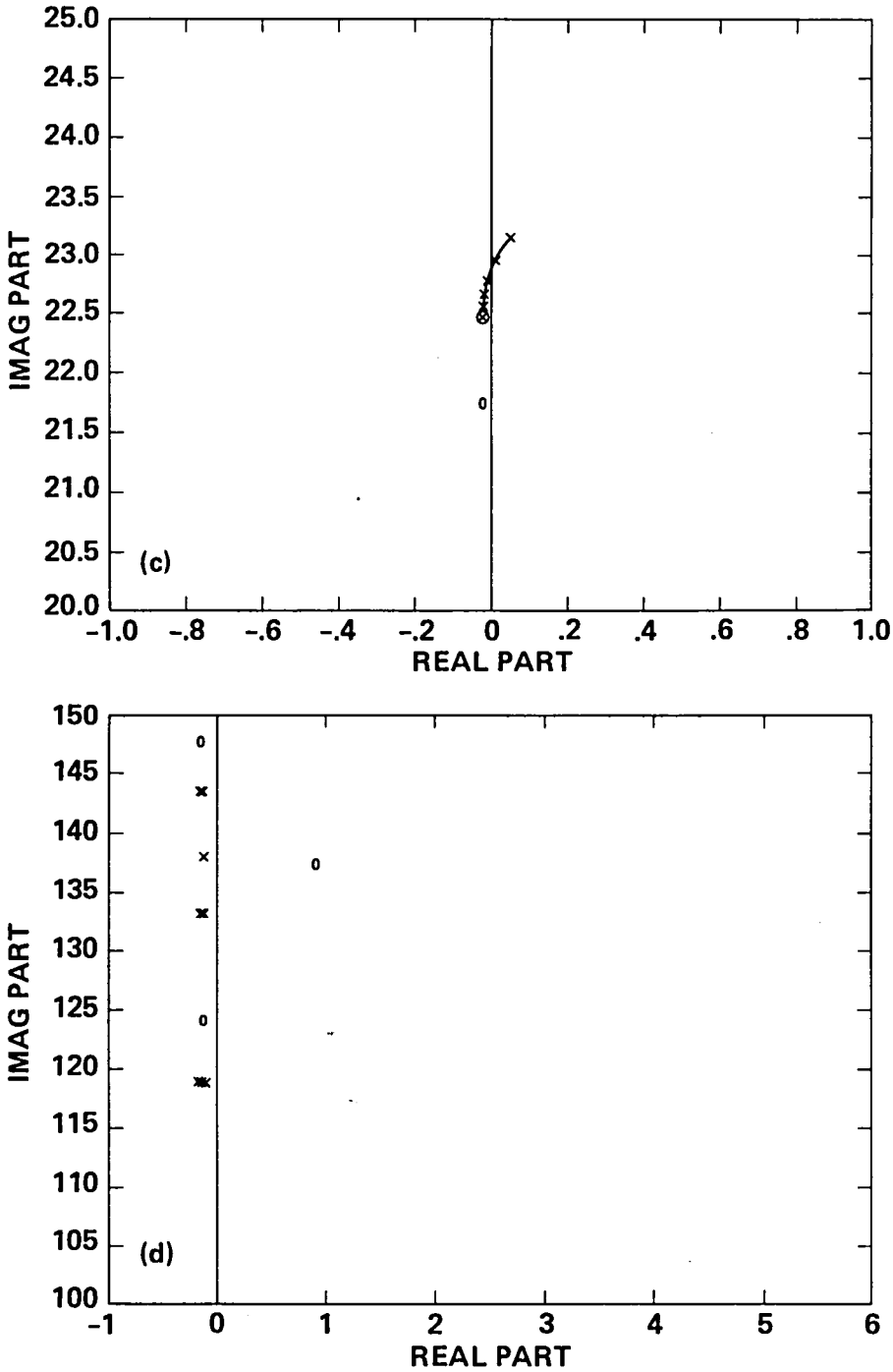

Figure 25.- Concluded. (c) The behavior of the 3.58-Hz mode. (d) Roots in the neighborhood of the 21.2-Hz bending mode.

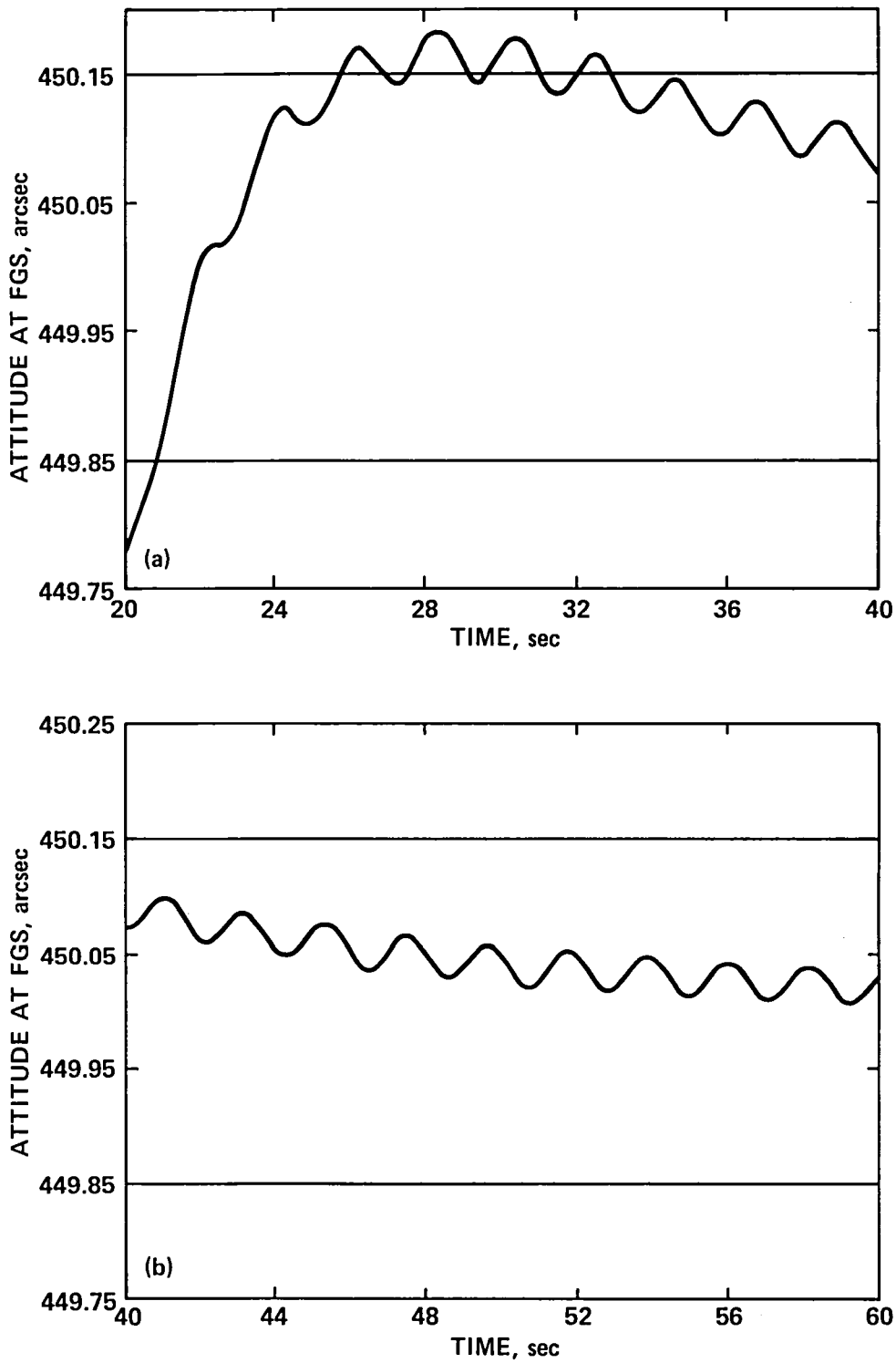

Figure 26.- Attitude response when the reaction wheel is placed at the CMG node, with no bending filter in the loop. (a) Settling to within 0.15 arcsec. (b) The residual oscillation.

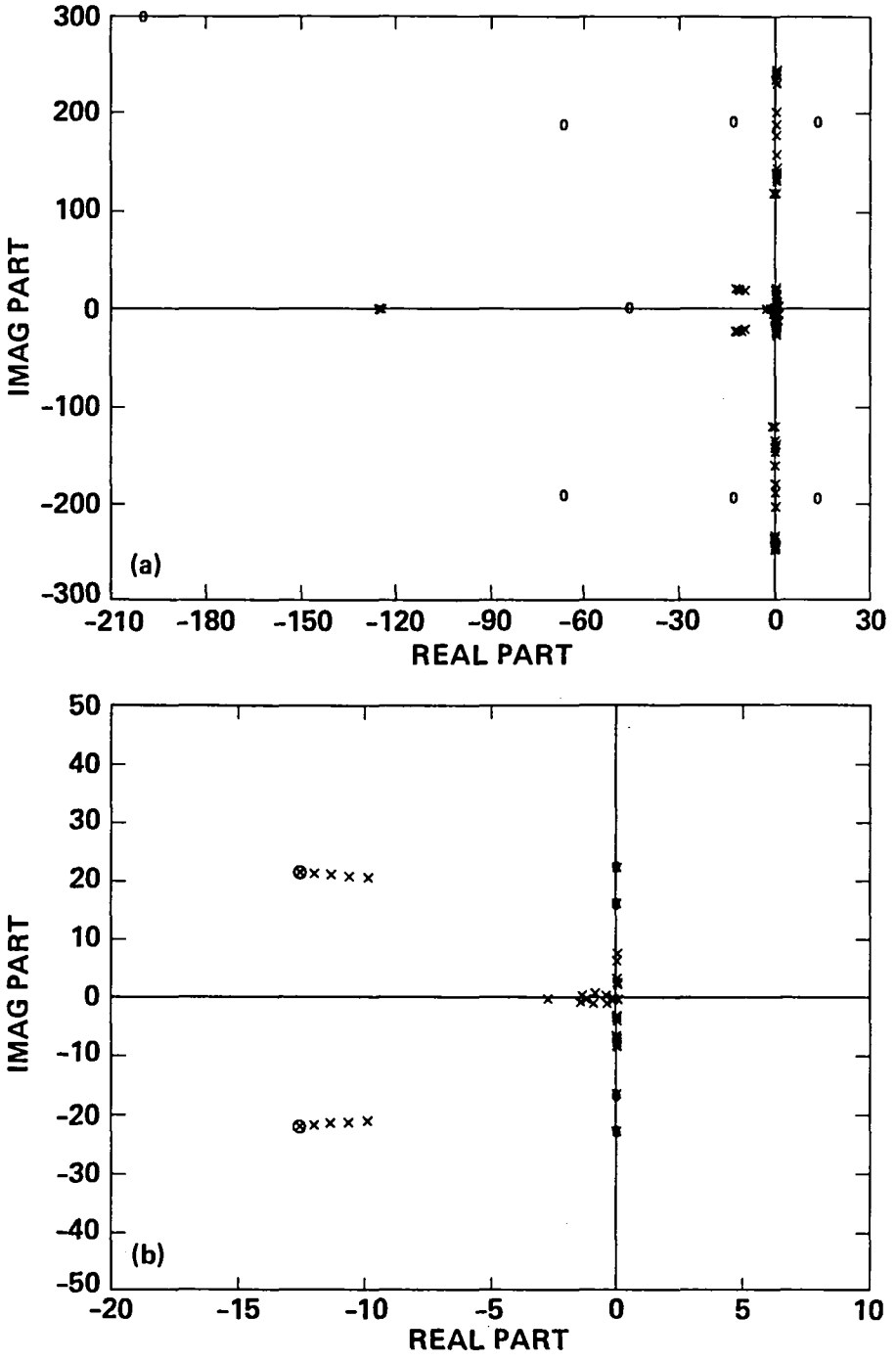

Figure 27.- Root-locus of the RIG loop with the reaction wheel moved to the CMG node and the RIG moved to the FGS node (no bending filter). (a) Overall picture including all modes. (b) Near the RIG poles.

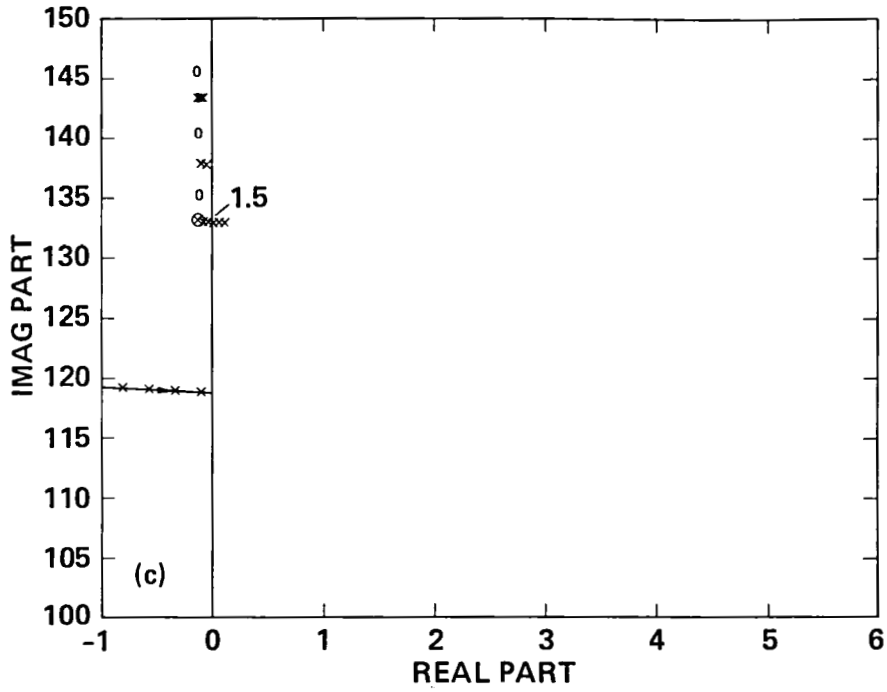

Figure 27.- Concluded. (c) In the neighborhood of the 21.2-Hz mode, showing instability for $K_f > 1.5$.

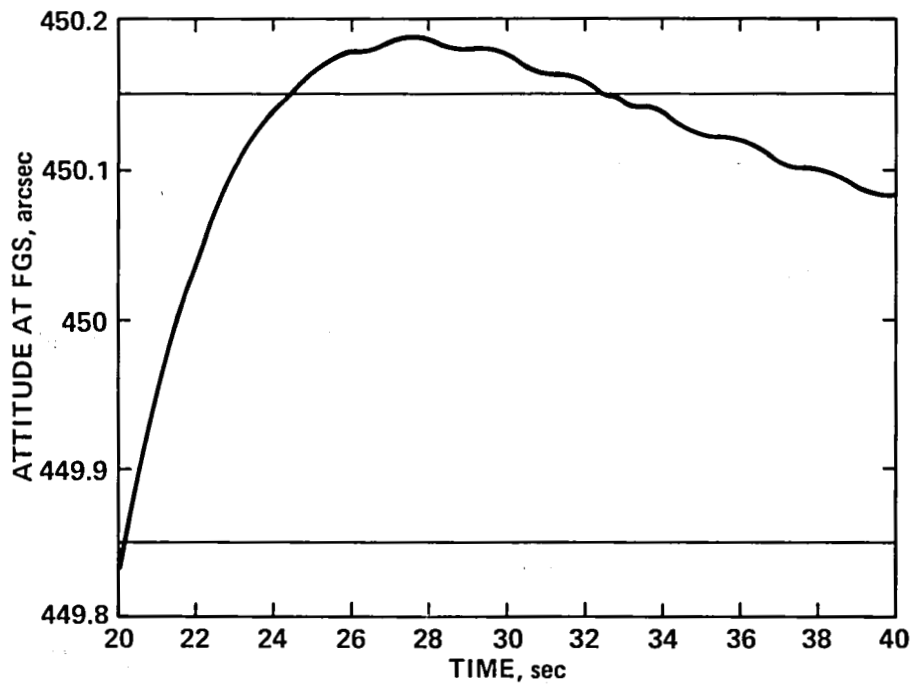

Figure 28.- Attitude response with the reaction wheel at the CMG node, RIG at the FGS node and no bending filter.

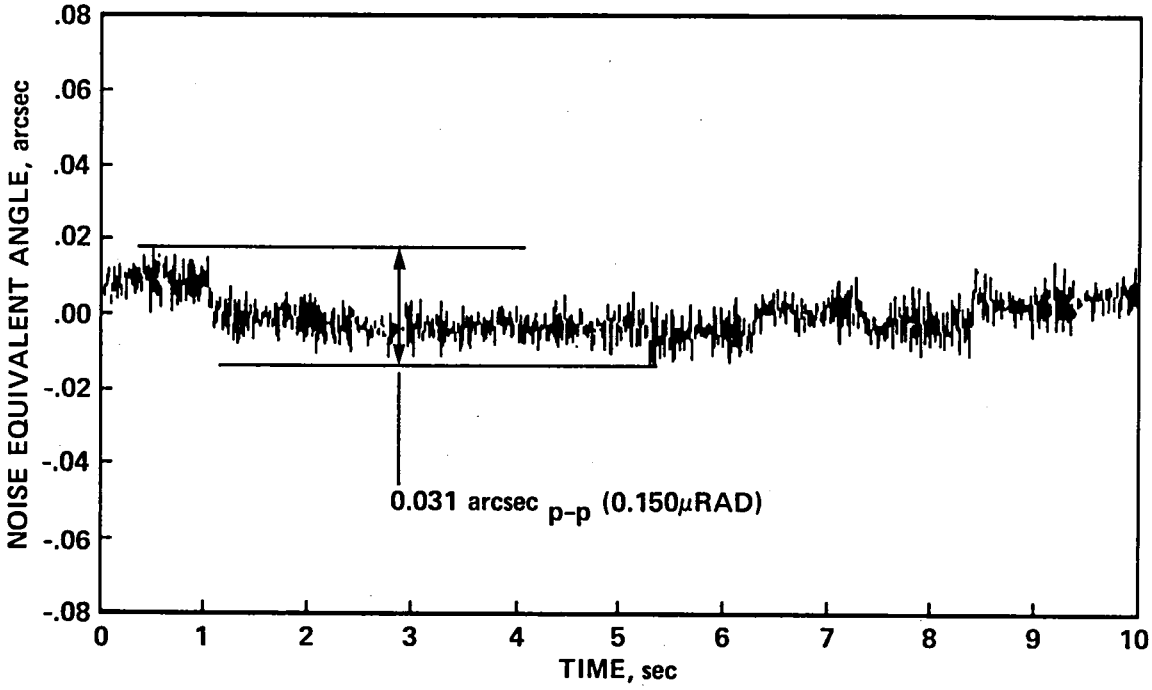

Figure 29.- Noise equivalent angle data for the RIG: a typical experimental result.

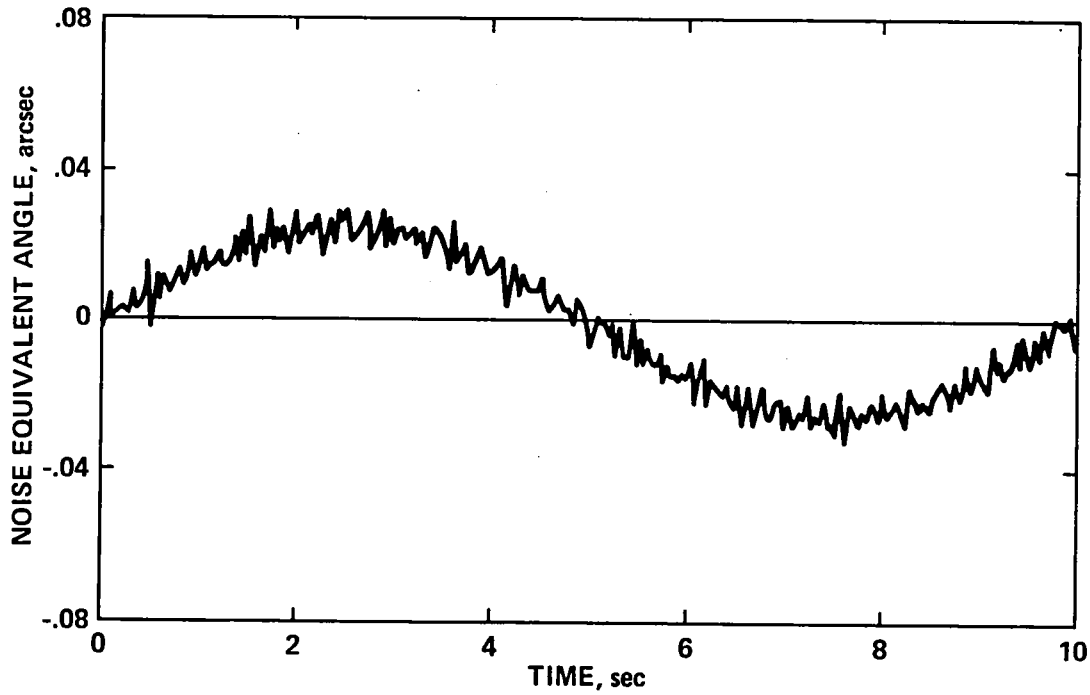

Figure 30.- Noise equivalent angle data generated for the simulation.

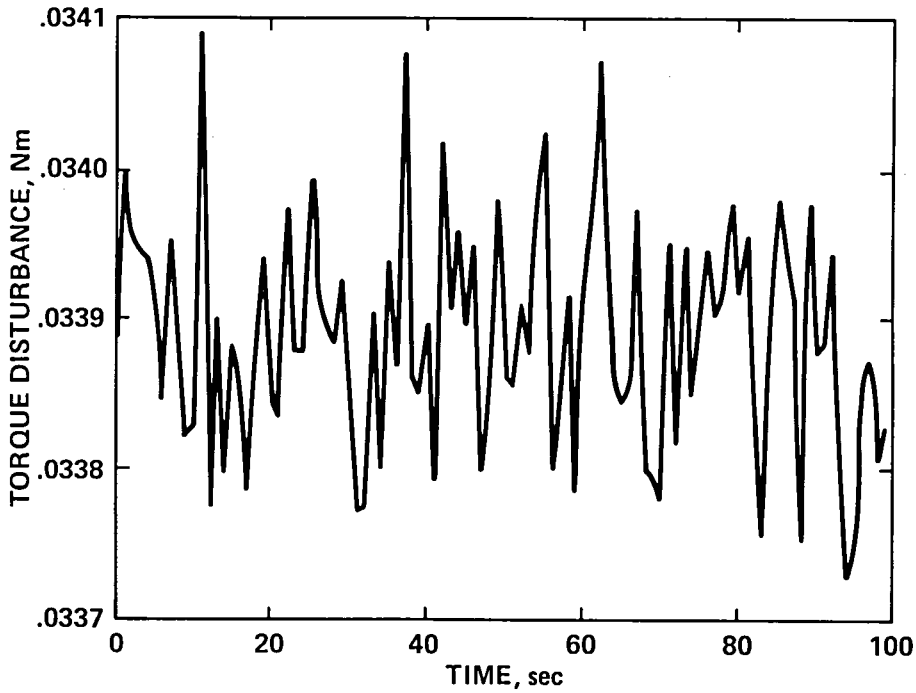

Figure 31.- Disturbance torques acting upon the observatory.

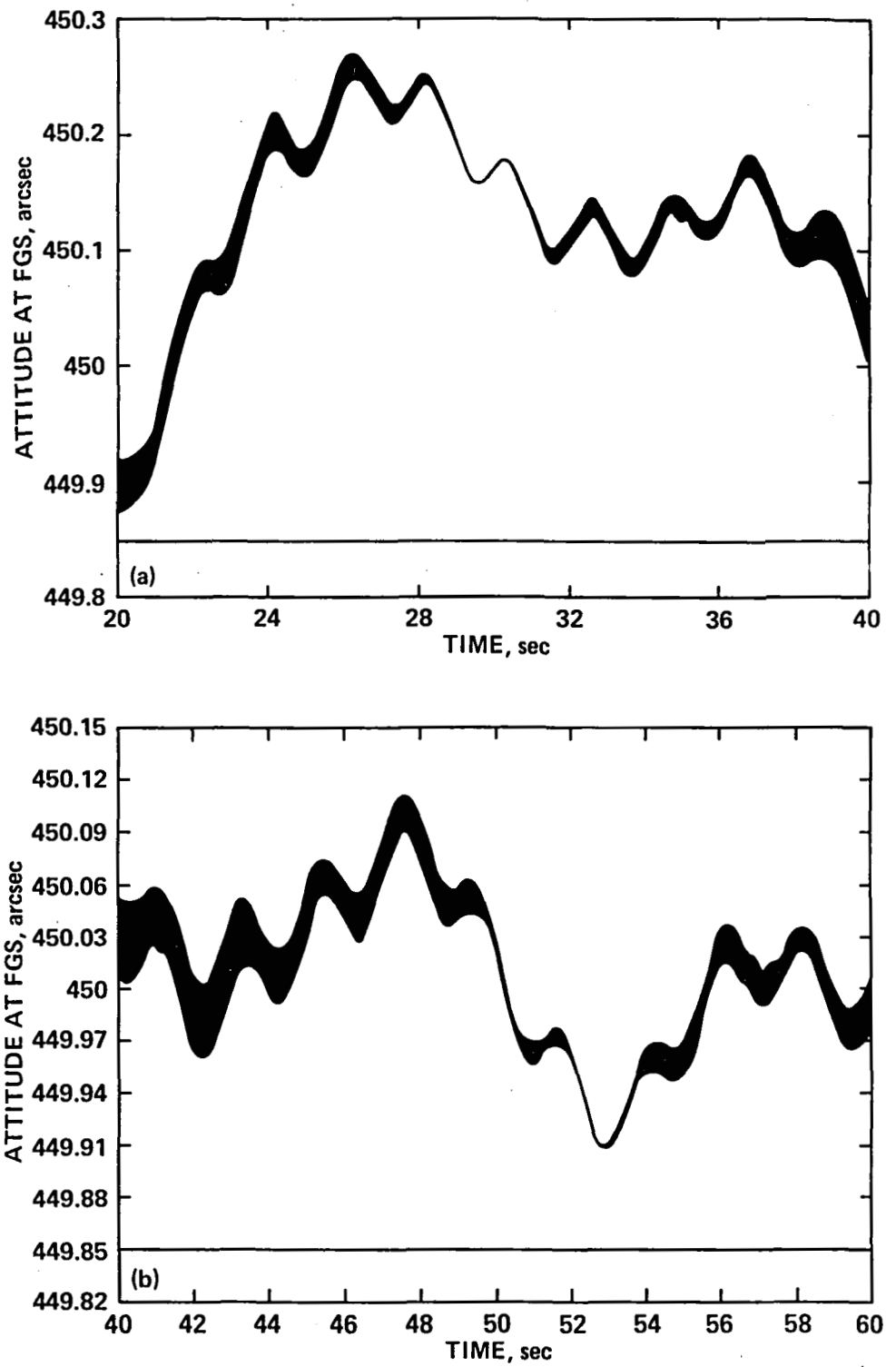

Figure 32.- Attitude response in the presence of disturbances. (a) The effect on settling time. (b) The steady-state response.

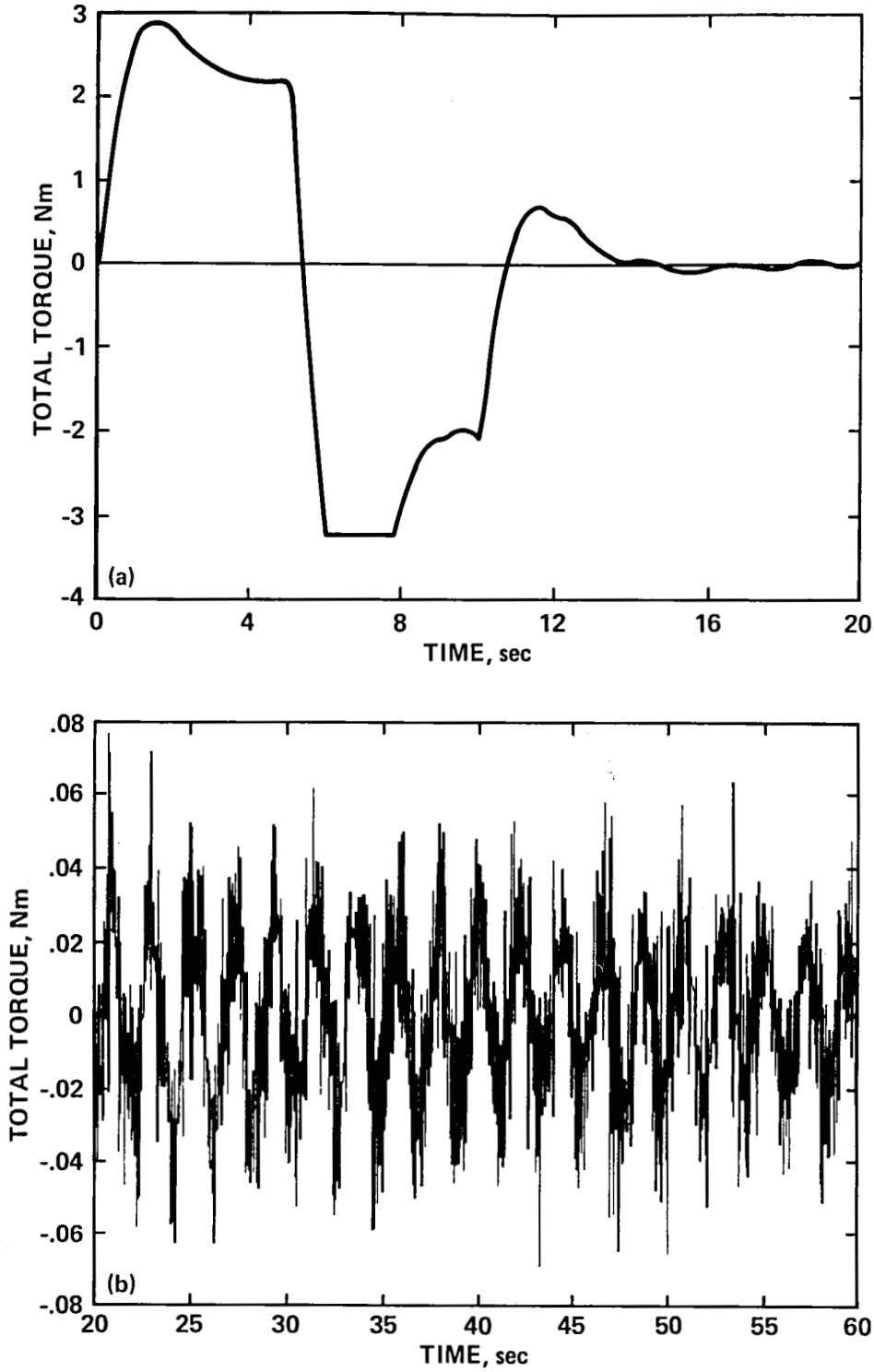

Figure 33.- Total torque exerted on the observatory during nod in the presence of disturbances. (a) During the slewing. (b) The quiescent torque shown magnified.

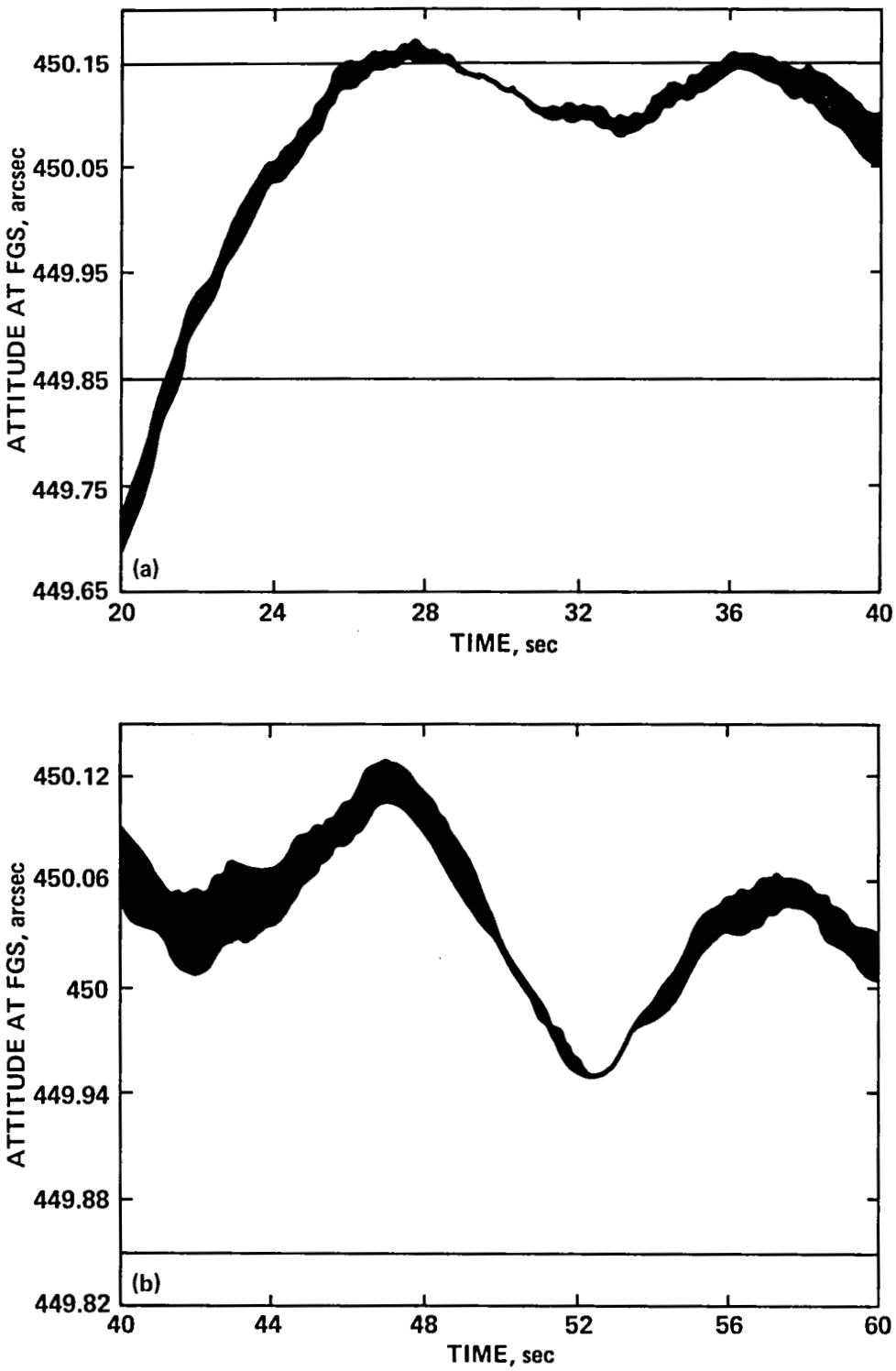

Figure 34.- Attitude response with a tilt-table actuator (maximum torque = 4.75 Nm), in the presence of disturbances. (a) Settling to within 0.15 arcsec of the commanded attitude. (b) Quiescent response.

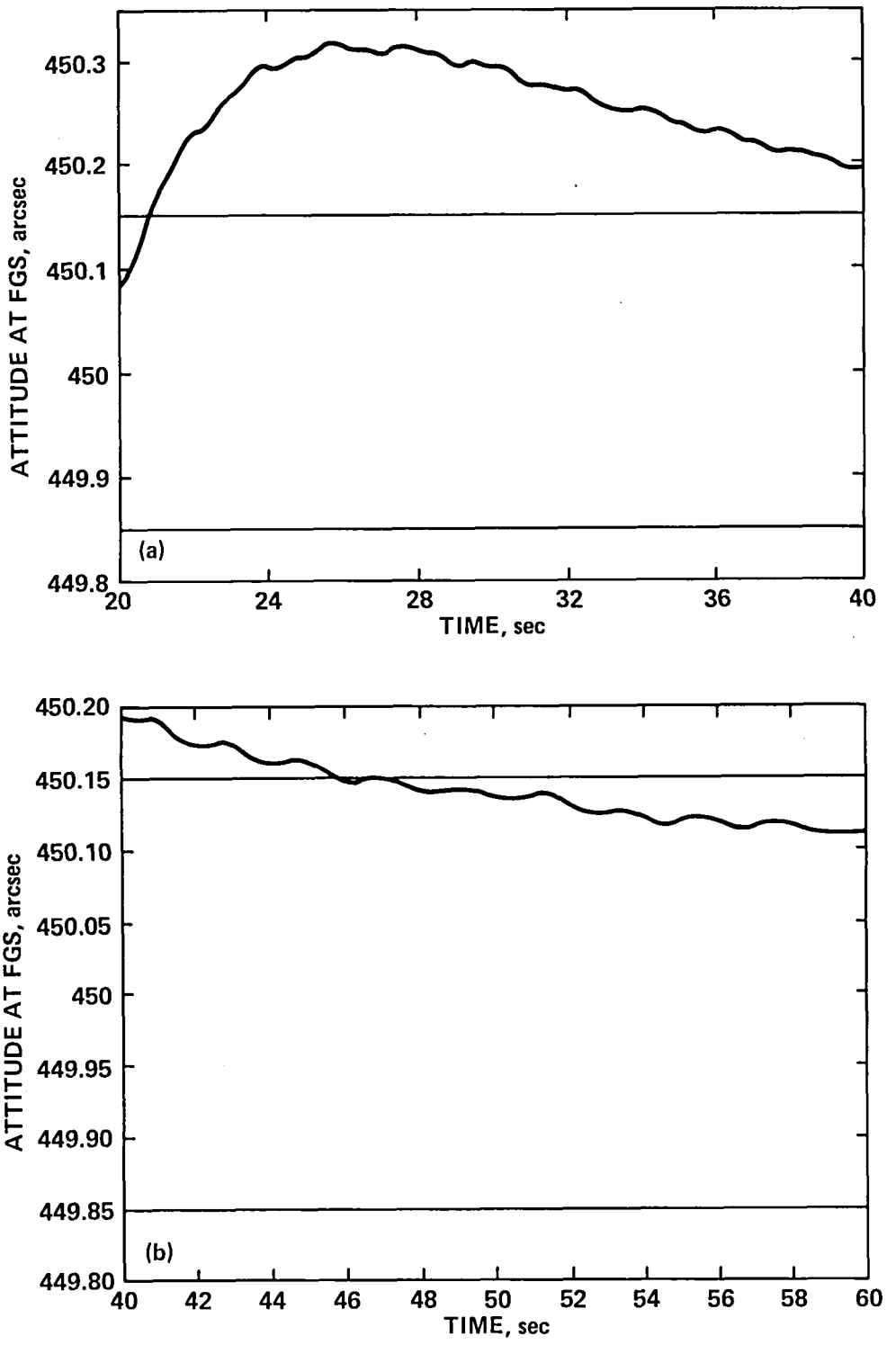

Figure 35.- Attitude response for a 9-sec duration triangular rate command without FGS in the loop. (a) Settling to within 0.5 arcsec in less than 20 sec. (b) Response slowly converges to commanded value.

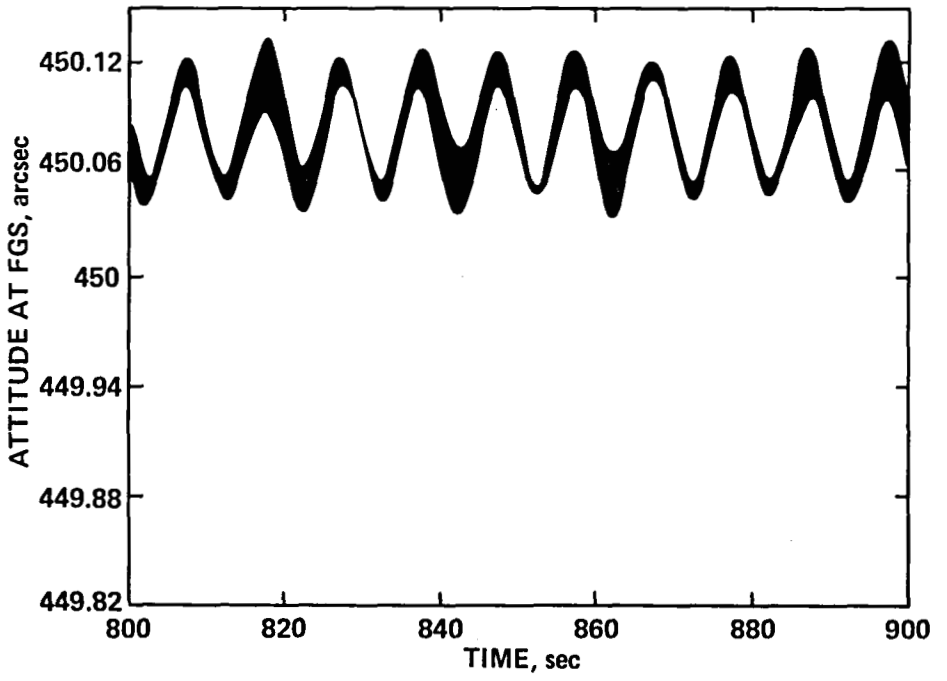

Figure 36.- Oscillation in the attitude response over the last 100 sec of a 900-sec observation period because of the RIG noise equivalent angle.

NASA
National Aeronautics and Space Administration

Report Documentation Page

1. Report No.	2. Government Accession No.	3. Recipient's Catalog No.
NASA TM-101007		

4. Title and Subtitle	5. Report Date
SIRTF Nod Maneuvers	August 1988
	6. Performing Organization Code

7. Author(s)	8. Performing Organization Report No.
N. Rajan	A-88202
	10. Work Unit No.
	159-41-06

9. Performing Organization Name and Address	11. Contract or Grant No.
Ames Research Center Moffett Field, CA 94035	
	13. Type of Report and Period Covered
12. Sponsoring Agency Name and Address	Technical Memorandum
National Aeronautics and Space Administration Washington, DC 20546-0001	14. Sponsoring Agency Code

15. Supplementary Notes

Point of Contact: N. Rajan, Ames Research Center, MS 244-10, Moffett Field, CA 94035
(415) 694-6520 or FTS 464-6520

16. Abstract

The response of the Space Infrared Telescope Facility's attitude control system to a nod command is studied under a wide variety of conditions. Several engineering issues are explored: the effects of variations in the structural model, relocation of sensors and actuators, the influence of the fine-guidance-sensor sampling period, resolution and noise on the system response, torque and rate-integrating gyro noise and disturbances. Simulation results using control-moment gyros and reaction wheels as actuators are presented.

17. Key Words (Suggested by Author(s))	18. Distribution Statement
Attitude control Simulation Maneuvers	Unclassified – Unlimited Subject Category: 18

19. Security Classif. (of this report)	20. Security Classif. (of this page)	21. No. of pages	22. Price
Unclassified	Unclassified	50	A03

For sale by the National Technical Information Service, Springfield, Virginia 22161